Bacterial Mechanosensitive Channel of Large Conductance (MscL) in Mammalian Cells for Novel Mechanobiology Applications

by

Johanna L. Heureaux-Torres

A dissertation submitted in partial fulfillment
of the requirements for the degree of
Doctor of Philosophy
(Mechanical Engineering)
in The University of Michigan
2018

Doctoral Committee:

Assistant Professor Allen Liu, Chair
Professor Gary Luker
Professor Edgar Meyhofer
Assistant Professor Sarah Veatch

Johanna L. Heureaux-Torres

heureaux@umich.edu

ORCID iD: 0000-0003-3410-3465

DEDICATION

This dissertation is dedicated to my mother, Ana, and younger siblings, Ulices and Aaliyha. Thank you for your support, inspiration, and love. ¡Los quiero mucho!

ACKNOWLEDGMENTS

The research detailed in this dissertation was funded by the NIH Young Innovator Award and NIH R21 CA198404 grant, and the University of Michigan, Ann Arbor Department of Mechanical Engineering. I was funded by the Rackham Graduate School Rackham Merit Fellowship (RMF), the NIH Microfluidics in Biomedical Sciences (MBSTP) training grant, the University of Michigan, Ann Arbor Department of Mechanical Engineering, and the Society of Hispanic Professional Enginers (SHPE) Graduate Dissertation Scholarship. I thank Dr. Boris Martinac for the *E. coli* MscL DNA constructs. Thanks to our direct research collaborators Professor Cheri X. Deng and Di Chen, PhD from the University of Michigan, Ann Arbor Department of Biomedical Engineering (Acoustic Tweezing Cytometry), and many members of the Luker Lab headed by Professor Gary D. Luker, M.D. and Kathryn Luker, PhD (*in vivo* mouse experiments and cell line development) in the University of Michigan, Ann Arbor Medical School. I thank Dr. Victoria L. Murray, Dr. Elisabeth Steel, and Dr. Luciana Rosselli-Murai, Dr. Lap Man Lee, Kenneth Ho, Arianna Brito, Yoani Herrera, and Danielle Chase (University of Minnesota) from the Liu Lab for helpful discussions and contributions. I also acknowledge the technical support from Lurie Nanofabrication Center (LNF) at the University of Michigan. Thank you to SHPE National, the National Graduate Committee, and SHPE University of Michigan chapter for their endless support and inspiration.

TABLE OF CONTENTS

LIST OF FIGURES

ABSTRACT

Mechanobiology, a relatively young field that centers on how external physical forces on cells or tissues and their intrinsic mechanical properties can influence physiology and disease, has become a pillar in cell biology. Indeed, cells experience a myriad of external, mechanical stimuli such as shear stress, stretch, substrate and matrix rigidity, surface topography, compression, and inter-cellular junction forces. Mechanosensors on the cell surface interfacing with the external environment (e.g., receptors, mechanosensitive ion channels, focal adhesions) and within the cell (e.g. the cytoskeleton) can sense, transmit, and amplify these inputs. This results in a cascade of intracellular biochemical signaling that leads to altered gene expression, protein expression, and finally, altered cell behavior and function. This process is known as mechanotransduction.

Mechanotransduction at the cellular-scale has perceptible, large-scale implications such as proper organism development, our ability to sense sound and touch, function and homeostasis of organ systems, and disease progression. Previous work in mechanobiology has focused on investigating or capitalizing on native, endogenous mechanotransduction. This dissertation work proposes a relatively unexplored frontier in mechanobiology: exogenous mechanotransduction, by demonstrating a novel approach towards achieving signal transduction and

mechanically driven behavior in cells through the introduction of exogenous mechanosensory components.

Here we demonstrate how the functional expression of the *E. coli* membrane tension gated mechanosensitive channel of large conductance (MscL) in mammalian cells endows the cells with new mechano-sensing capabilities such as the activation of MscL in the plasma membrane through membrane tension resulting from (1) osmotic down-shock and (2) new interactions with native mechano-sensory components, as well as altered cell function such as (3) impairment of cell migration in metastasis *in vivo* and narrow, 3D confinement *in vitro.*

The first major contribution in this thesis was to show that MscL can be expressed in mammalian cells, localize to cellular membranes, and responds to membrane tension via osmotic down-shock. The second contribution was demonstrating that the activation of the bacterial MS channel expressed in mammalian cells can be mediated through localized membrane stress that is dependent on the native actin-cytoskeleton. This was done by using acoustic tweezing cytometry (ATC) where acoustic excitation of microbubbles targeted to surface integrin receptors generated localized forces that robustly gated MscL. Impermeable, fluorescent dye uptake was used to report MscL activation; also showing that activated MscL can deliver large molecules into the cell.

Lastly, we investigated the effect of MscL mechanotransduction on the cell function of migration in cancer metastasis and then more specifically, 3D-confinements. Our findings in our *in vivo* mouse model showed that there was a

marked reduction in metastasis to the lung for MscL expressing cancer cells compared to controls. *In vitro* migration experiments using a biomimetic microfluidic device revealed that MscL activation due to 3D-confined migration could be responsible for the observed reduction in metastasis. We found that ~46% of MscL-expressing cancer cells that entered extremely narrow confinements of 30 μm^2 cross-section had activated MscL and only 11% of these cells were able to fully enter the channel and migrate.

Implications of this thesis are that MscL: (1) can be used as a molecular delivery tool for live-cells via mechanical stimulus; (2) can provide insight into the metastatic cascade and mechanobiology focused therapies; and (3) in mammalian cells can serve to study existing mechanotransduction or potentially engineer new mechanical properties and signaling in cells.

CHAPTER I

Background, Motivation, & Research Objectives

This thesis is in the field of mechanobiology and demonstrates for the first time exogenous mechanotransduction in mammalian cells through the novel approach of functional expression of an exogenous, bacterial mechanosensor, mechanosensitive channel of large conductance, (MscL). In this chapter background and motivation on mechanobiology, mechanotransduction, and MscL is provided. To-date mechanobiology has primarily focused on endogenous mechanotransduction leading to many technological advancements and significant amassed knowledge. This has set the stage for moving into the unexplored area of exogenous mechanotransduction and engineering mechanotransduction for attractive mechanobiology applications. To achieve this goal, bacterial MscL was identified as a suitable mechanosensor.

Mechanobiology and Mechanotransduction

Mechanobiology, a relatively young field, centered on how physical forces on cells or tissues and their intrinsic mechanical properties can influence physiology and disease, has already become a pillar in cell biology. Indeed, cells experience a myriad of external, mechanical stimuli such as shear stress, strain, substrate and matrix rigidity, topography, osmosis, compression, and inter-cellular junction forces (Figure

1.1). Mechanosensors on the cell surface that interface with the external environment, including receptors, mechanosensitive ion channels, protein complexes such as focal adhesions, and within the cell, such as the cytoskeleton, can sense, transmit, and amplify these inputs. This results in a cascade of intracellular biochemical signaling that ultimately leads to altered gene expression, protein expression, and finally, a change in cell behavior and function. This process is known as mechanotransduction.

Mechanotransduction occurring at the cellular-scale has perceptible, large-scale implications such as our ability to sense sounds and touch, the proper functioning of organ systems, interpretation of key external cues for organism development, and disease progression. This has motivated researchers in recent decades to reach many milestones in mechanobiology (Figure 2). Significant discoveries include that of the integrin family proteins[1, 2], mechanosensitive channels in bacterial cells via patch clamp experiments [3, 4], control of stem-cell differentiation and proliferation into various cell types by tuning substrate stiffness [5-7], linking human genetic disorders to defective mechanosensors such as anemia xerocytosis resulting from a mutation in mechanosensitive channel Piezo [8], and differences in cancer and diseased cell deformability compared to healthy, somatic cells allowing for mechanical phenotyping [9, 10].

Mechanobiology is at the intersection of biology and engineering, which is evident as it focuses on physical forces on biological systems; but this is also evident in many of its breakthroughs that consist of discoveries tightly coupled to technologic-

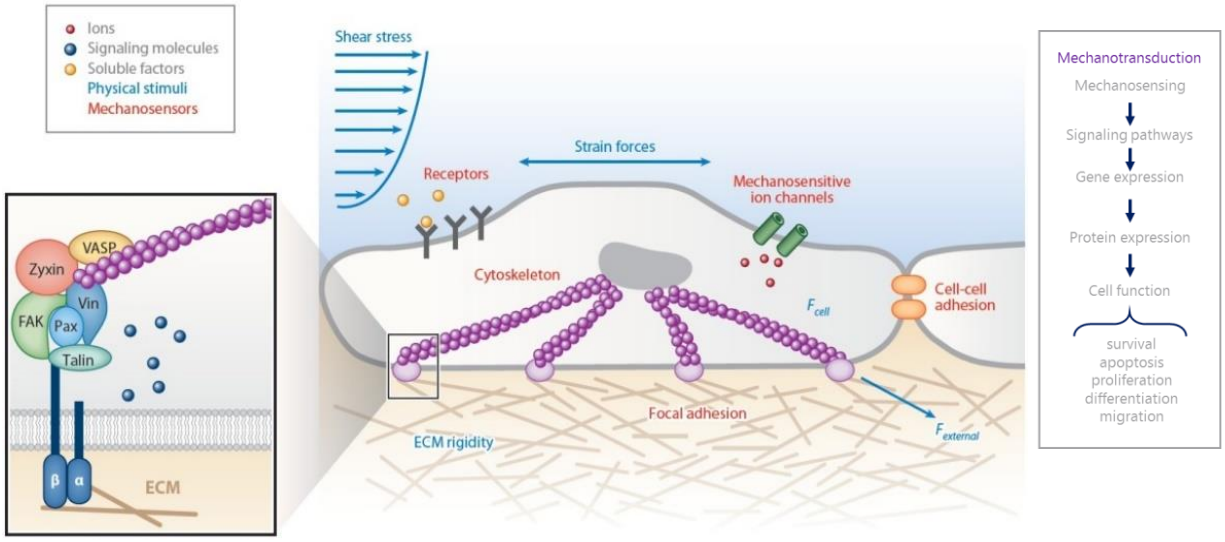

Figure 1.1 Diagram Summarizing Mechanobiology of a Single Cell. Left: image legend; and a close-up view of a focal adhesion that binds to the ECM via integrins and assembles an intracellular protein complex that connects to the cell cytoskeleton. Center: a cell with representative physical stimuli and mechanosensors. Right: mechanotransduction cascade (adapted from Sun *et al.*, 2012) [11]

-al advancements and application of state-of-the-art tools [12]. Technological advancements, many borrowed from engineering applications, such as variable stiffness silicone substrates [5, 13], traction force microscopy [14], optical tweezing cytometry and atomic force microscopy [15, 16], super-resolution imaging [17, 18], and microfluidic devices [19, 20] have opened previously inaccessible lines of inquiry.

Though these milestones span various mechanosensors, cell functions, signaling pathways, and technologies, all have focused on investigating or capitalizing on native, endogenous mechanotransduction. We have reached a point in our amassed mechanobiology knowledge where we can begin to engineer novel mechanotransduction to further our understanding and open new paths toward innovation. In this thesis, we propose moving into this relatively unexplored frontier in mechanobiology and show a logical approach to achieving the goal of engineering

novel signal transduction and mechanically driven behavior in cells through the introduction of exogenous mechano-sensory components.

We focus on using the *E. coli* mechanosensitive channel of large conductance (MscL) as the exogenous mechanosensor. MscL is a membrane tension activated channel protein that has no direct homolog in mammalian cells and thus has many unique attractive mechano-sensing features not typical in mammalian cells. This, coupled with the fact that MscL is the best studied MS channel to date make MscL highly suitable for achieving novel mechanotransduction in mammalian cells.

Mechanosensitive channel of large conductance (MscL)

Introduction: Mechanosensitive (MS) channels are a class of dynamic, mechanically gated molecules and are among the best-characterized force-sensing systems. MscL was first identified in 1987 from early electrophysiological studies of giant *E. coli* spheroplasts [4]. This along with other early observations demonstrated that these MS channels were activated by pressure, had large conductance, and resided on the inner, cytoplasmic membrane of *E. coli* [3]. It was hypothesized that MscL functions as an "emergency release valve", protecting cells from lysis under turgor pressure.

mscL Gene, Crystal Structure, and Protein Reconstitution: To study MscL in depth, the mscL gene encoding for the protein needed to be ascertained. The identification and cloning of the mscL gene was a tremendous feat, requiring the use of unconventional methods such as reverse cloning (i.e., working backward from

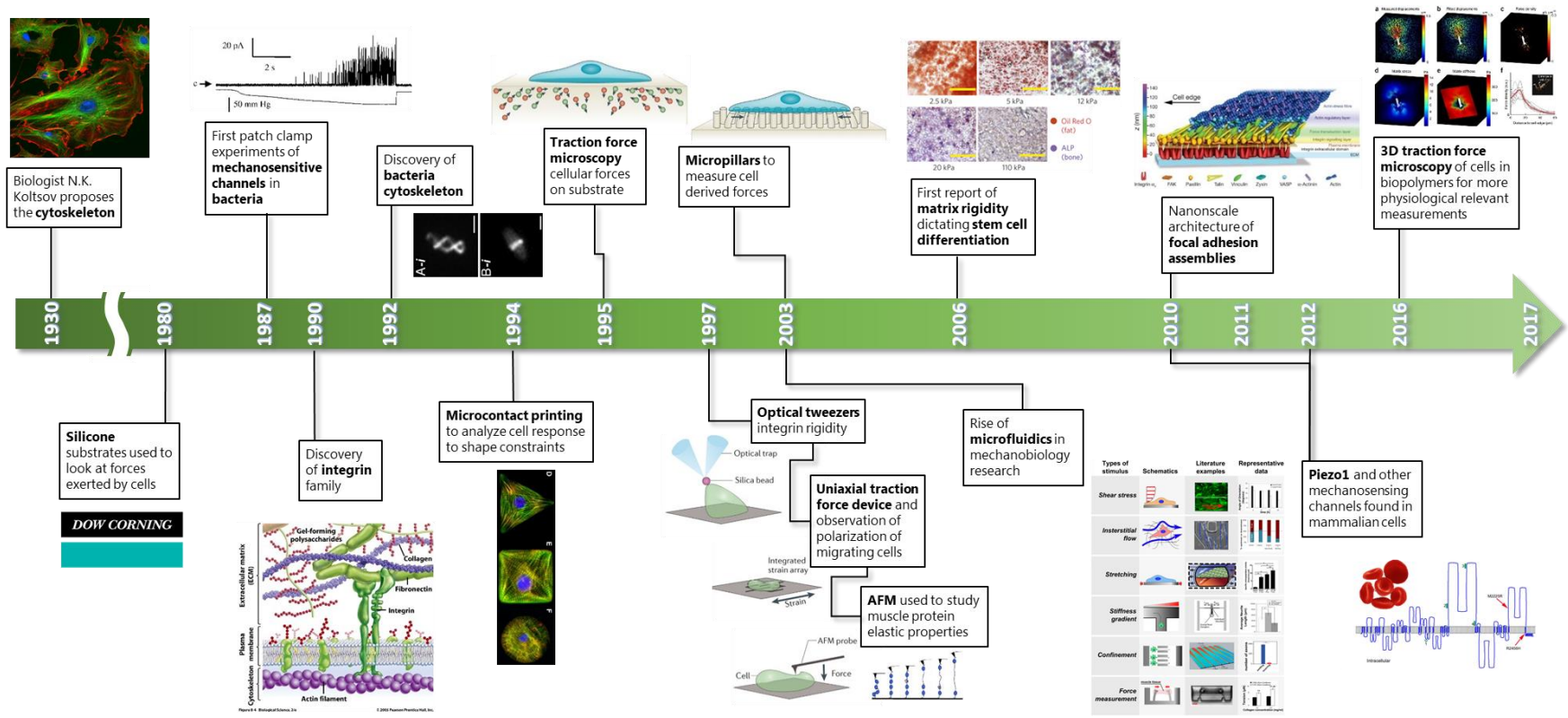

Figure 1.2 A Timeline of Mechanobiology. Timeline depicts a small sampling of key breakthroughs made in the field of mechanobiology starting from the early 20th century. [12]

protein to gene). To acquire the MscL protein, numerous steps of patch clamp functional assaying followed by fractionation then followed by reconstitution into liposomes were performed until obtaining an MscL-only fraction [21].

This allowed researchers to independently reconstitute MscL into proteoliposomes (i.e., purified proteins reconstituted into liposomes); and further patch-clamp experiments on these systems determined that MscL functions independently from other proteins or molecules and is exclusively gated (or opened) by membrane tension [22]. Patch clamp characterization of MscL determined its gating threshold tension to be close to 10.4 mN m^{-1} [23].

The MscL protein crystal structure was determined from *M. tuberculosis* and *S. aureus* [24, 25]. Based on those structures, the *E. coli* channel is predicted to have a pentameric configuration, with five symmetrically arranged subunits about the channel pore [26, 27] (Figure 3). The subunits consist of two transmembrane domains (TM1 and TM2), N- and C-terminal cytoplasmic domains, and a periplasmic loop. The channel has a funnel shape, with the larger opening lined by TM1 and facing the periplasmic surface, and the narrowest point facing the cytoplasm, plugged by hydrophobic residues Leu19 and Val23 [28, 29].

Structure-Function Relationships: After MscL's discovery, gene isolation, and determination of its crystallographic structure, researchers began to probe into MscL domains structure-function and the channels gating mechanism. An early study on structure-function focused on the contributions of the extra-membranous domains of

the channel (i.e., N-terminus, C-terminus, and periplasmic loop) to the channel activity and did so by utilizing specific proteolysis. Using an excised patch clamp-

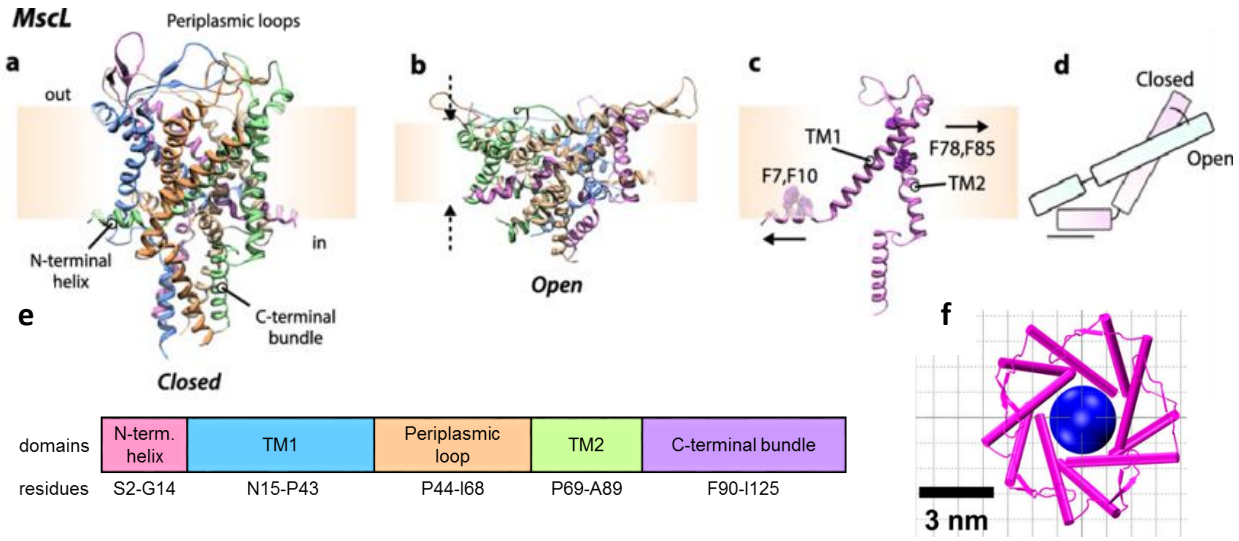

Figure 1.3 MscL Structure. (A) Ribbon model of closed MscL channel protein side view with subunits denoted by different colors and some protein domains labeled embedded in a lipid membrane (light orange band) (B) side view of MscL channel in the open configuration, membrane is under tension and thinner (C) A single subunit view under membrane tension. Key residue-membrane anchors shown with respective applied forces on the N-terminal and TM2 domains. (D) Simple diagram of the tilting of the TM1, inner pore domain during channel gating. As the N-terminal anchor is pulled, it transmits force along TM1, aligning TM1 into a continuous helix and opening the channel pore. (E) List of all MscL subunit domains and respective amino acid residues. (F) Top view of open MscL channel showing a maximum pore size of 3 nm. (Adapted from Martinac and Cox, 2016 and Wang *et al.*, 2014 [30, 31])

mode on single channels, the researchers claimed they were able to selectively expose the cytoplasmic facing side or periplasmic facing side of the channels to protease. For the C and N-termini, proteolysis showed an increase in the mechanosensitivity of the channel without changing its conductance [32]. In contrast, after cleavage of the periplasmic loop for each monomer, the channel was still functional with dramatically increased mechanosensitivity. The loop does this by acting as a spring that resists the opening of the channel and helps MscL's closure when it is open. It must be noted that the effect of proteases trypsin or chymotrypsin was only observed when the channel was gating, indicating that its opening exposed the periplasmic loops'

protease-sensitive sites. Also, to note is that due to the lack of precision of the proteolysis, it is not known what the exact deletions were on these domains. For the N-terminus it can be assumed that at least the deletion of the first 7-10 amino acids (i.e., up to the Phe residues) resulted in increased sensitivity. Together these results indicate that the integrity of most of the extra-membranous domains is not necessary for mechanosensitivity. They instead suggest that they counteract the changes of the transmembrane helices and potentially set the level of sensitivity of the channel to tension.

A more precise explanation of MscL's N-terminal function was recently revealed using finite element (FE) and molecular dynamics (MD) simulations in conjunction with spin-labelling and electron paramagnetic resonance (EPR) spectroscopy [33]. The N-terminal domain is a 14-amino acid long amphipathic helix that aligns with the membrane-cytoplasmic interface. It acts as an anchor and stabilizes the MscL's closed state. When the lipid bilayer is stretched, the N-terminal helix is pulled along the direction of the surrounding lipids and consequently transmits force from the Gly4 residue to the end of TM1. TM1 then aligns with the N-terminal domain and forms a continuous helix (Figure 3d). The addition of amino acid residues to the N-terminus was found to not affect channel activity, however deletions or changes to the N-terminal amino acid sequence results in altered pressure sensitivity and gating; additions of flexible glycines at the Gly-4 site led to an increase in the pressure required for MscL gating [28, 33]. Deletions led to loss of sensitivity channel phenotypes where expression of these constructs could not rescue

E. coli from hypo-osmotic shock. The most severe loss of sensitivity was seen with a Δ2–7 deletion construct, requiring much more force to gate when probed using patch-clamp electrophysiology. The N-terminal helix of MscL acts as a critical structural element in tension-induced gating, both stabilizing the channel's closed state and coupling the channel to the membrane. The N terminus is an essential driver of orienting the TM1 domain and the radial expansion of the channel pore [33, 34].

Similar FE and MD simulation coupled spectroscopic experiments were done for the 36-amino acid long C-terminal [35]. The results confirmed that in the MscL closed pore configuration, the subunit C-terminals form a bundle of five, hydrophilic α-helices concentric with the channel transmembrane bundle and collinear with its axis of symmetry (i.e., axis through the channel pore, from the cytoplasm to the periplasm). During channel gating, a top section of the C-terminal domain, A110-E118, dissociates and the remainder of the C-terminus does not change orientation. This implied that the C-terminus serves as a molecular sieve and stabilizer of the oligomeric MscL structure. Despite the C-terminus function, deletion of 27 amino acids from the C-tail does not alter MscL gating in response to pressure, however, deletion up to 33 amino acids causes MscL to not activate [28]. Those C-terminal amino acids at these sites, 104-108, consist of a highly-conserved cluster, RKKEE, among many different MS channels [36]. This conserved region functions as a proton sensor of the external environment by adjusting the channel sensitivity to membrane tension in a pH-dependent manner by altering the C-terminus orientation. Protonation of the basic and acidic chains of residues within the RKKEE charged

cluster by a decrease in pH may prevent the channel from opening and led to considerably higher pressure threshold for channels in liposomes [36].

Later random and scanning mutagenesis of the *mscL* gene, showed that when a hydrophilic amino acid replaces one of the hydrophobic residues on the upper interface between the membrane lipid and the channel's periplasmic end of the transmembrane domains, TM1 or TM2, MscL is unable to open in response to membrane tension. Loss-of-function mutants have been isolated in the periplasmic loop [37]. This change in the sensitivity was suggested to be due to a change in the folding and/or stiffness of the loop since through proteolytic digestion of the loop it was shown to increase the mechanosensitivity [32]. In TM1- and TM2-loop mutants (V37D, I40T, P69L, and M73K) no channel opening or high threshold activation was observed. Residues near the end of TM2 (Phe78, Ile79, Phe83, and Ile87) and TM1 (Leu36, Ile40, and Ile41) mutated with hydrophilic asparagine also lead to lower viability and much higher gating threshold suggesting that these sites receive the membrane tension from the surrounding lipid through hydrophobic interaction. Despite complementing these mutants with TM1 G22X mutants, which were shown to increase channel sensitivity, the function of MscL is severely impaired as shown in liposome patch-clamp experiments and *in vivo* hypoosmotic-shock [37]. Hydrophilic substitution of other residues at this lipid-protein interface did not impair MscL's mechanosensitivity. Disturbing the hydrophobic interaction between the membrane lipid and the channel's periplasmic funnel rim, impairs the function of MscL [37].

Gain of Function Mutants: Other random mutagenesis of the TM1 domain, the pore-lining helices, had an opposite effect to MscL mechanosensitivity [29]. Instead, gain of function (GOF) MscL mutants (i.e., mutants with greater sensitivity and lower gating threshold compared to the WT), were discovered [29]. These mutants in *E. coli* were classified into groups of severity that showed increasing leakage of solutes and decreasing cell viability. The most severe mutants were found to be on residues Gly22, Val23, Gly26, and Gly30. The open probability of the MscL channel as a function of applied pressure as determined through patch clamp experimens showed that the GOF mutants retain the shape and slope of the WT probability curve but was shifted left towards lower pressures indicating the mutants have lower activation pressure threshold but the "spatial" gating parameters were not change. The kinetics for GOF mutants also differed from WT, where the severe mutants had flickering channel activity and open dwell times less than 1 ms as contrasted by WT, which can have major open dwell times tens of milliseconds. This result indicated that GOF mutants have a lower transition barrier between open and closed states [29].

Among those previously probed residues, Gly22 is highly conserved in other bacterial MscL homologues. In the previous known MscL structure from *Mycobacterium tuberculosis* [24], Gly22 was buried within the constriction within the closed channel pore. In order to elucidate the molecular mechanism of the channel gating, one study substituted Gly22 with all other common amino acids [38]. Substituting of Gly22 with hydrophilic residues decreased the threshold pressure at which channels opened. The channel open probability distribution as a function of

pressure for the MscL channels were compared to that of the mechanosensitive channel of small conductance (MscS). MscS is also expressed in *E. coli* and is known to function similarly to MscL except for having a lower activation threshold, smaller conductance, and thus typically activating before MscL in response to membrane tension [39-41]. Due to variation in micropipette dimensions in patch experiments, MscS was used as an internal control. MscL activation threshold was 1.64x greater than that of MscS [42]. The MscL severe GOF mutations listed starting with the most severe as N-Asn (e.g., can be activated with no applied pressure), E-Glu, D-Asp, R-Arg, K-Lys, Q-Gln (e.g., threshold of 0.4x that of MscS), and H-His caused a significant decrease in bacterial growth rate and pressure gating threshold. More moderate GOF mutants were S-Ser (1.14x MscS threshold) and T-Thr. Channel kinetics also varied with hydrophilicity. G22S and G22T exhibited flickering with dwell events close to 2 ms. The severe GOF mutants exhibited flickering activity at open dwell times closer to 0.5 ms in addition to a stable substrate near or at the lowest sub-conductance level of MscL WT of 0.5 nS. MscL has been shown to have multiple sub-conducting states between the fully-closed and fully-open states [42]. These mutants had two activation thresholds and activation probability for lower applied pressure range, which led to transitions from the closed state to the more favored sub-conducting state, and higher applied pressure range, which led to transitions from the sub-conducting state to a more favored fully-open state [38].

Indeed, the TM1 has been shown to be the channel gating hotspot and alterations to these amino acids confer the MscL channel chemical gating. GOF

mutants such as G22S have been show to require half of the tension needed for activation at ~5-6 mN/m while other mutants such as G26C have the added advantage of being chemically gated using small reducing agents such as 2-(trimethylammonium) ethylmethanethiosulfonate bromide (MTSET) [43, 44]. Cysteine scanning of the channel, has revealed residues G26, G30, and S34 on TM1, forming a vestibule in pore of the channel closed structure, to produce a phenotypic change when exposed to MTSET alone. In particular, G26C mutated channel upon periplasmic exposure of 2 mM MTSET spontaneously activated, initially sporadically residing at multiple sub-states and over a matter of a few seconds becoming "locked" into an open sub-state ~4/5th the fully-open state.

MscL Gating Mechanism and Conducting States: Understanding the locations and gating effects of MscL's residues have helped researchers produce a clearer mechanism of the channel gating, pore dimension, and lipid interactions. MscL is gated by tension transmitted through the lipid bilayer. Using purified MscL reconstituted in liposomes, researchers have been able to study single channel currents as an applied pressure (p) is varied and thus the lipid membrane surface tension (T) altered [42]. Video microscopy during patch experiments allowed for the calculation of tension by knowing p and the radius of curvature of the liposome in the patch pipette. MscL channel activity is often described in terms of its open probability (P_o), which has a has a steep sigmoidal dependence on T, with a midpoint ($T_{1/2}$) of 11.8 dyn/cm (or 11.8 mN/m) [42]. MscL WT has shown a maximal slope sensitivity of P_o/P_c (where P_c is the closed probability) as 0.63 dyn/cm per e-fold (i.e., time interval in

which an exponentially growing quantity increases by a factor of e). It terms of energy, the channel state probabilities follow a Boltzmann distribution and the energy difference between the closed and fully open states is $\Delta E = 18.6 k_B T$. Equating this free energy to spatial parameters, $T\Delta A$, where (ΔA) is the change in the in-plane area, gives $\Delta A = 6.5$ nm^2.

MscL is not a binary channel, but has an additional four states. These are achieved sequentially as C↔CE↔S1↔S3↔O, where C, CE, S, and O refer to the closed, closed expanded, sub-conductance, and open states, respectively [26, 27, 42]. The transition from the closed to closed expanded conformation produces no conductance and is elastic. When the expansion of the channel rim places sufficient stress the channel first opens to a sub-conducting state, S1. The tension dependency of transition from the CE to S1 suggested that there is an in-plane area increase, ΔA, of ~4 nm^2, 2/3rds of the closed to open state ΔA. Low sub-conducting (S1) and fully-open (O) state transitions are relatively independent of tension [26]. In order to explain the closed expanded state, a model was developed in which the N-termini of the channel act as a second gate [26, 42]. This model has since been proven incorrect and the N-terminal helices have been shown to act as a dynamic membrane coupling element that associates with the bilayer at the cytoplasmic interface and drives the tilting of the pore-lining TM1 helix [33, 34].

The importance of the interactions of MscL and the membrane is supported by the observation that variations in the phospholipid bilayer thickness or the addition of compounds that induce membrane curvature such as lysophosphatidylcholine

(LPC) directly impact the tension required to gate MscL [45, 46]. Thus, membrane deformation and tension can be perceived by MscL as a hydrophobic-mismatch at the protein-lipid interface, where the opening of the channel results in a favorable reduction in free energy. The details of the protein conformational change were worked out by Wang *et al.* by using single molecule FRET (smFRET) of MscL in reconstituted liposomes [31]. They were able to (1) demonstrate that the conformational change of MscL during gating follows a helix-tilt mechanism, (2) report measurements of the distance changes on MscL transmembrane α-helices and (3) directly observe that the open pore reaches 2.8 nm in diameter. In addition, based on the measurements, they developed a molecular dynamics model of the channel structure in the open state which confirmed their experimental findings.

Unique Advantages and Limitations: These MS channels are predicted to exist in all three kingdoms of life [47]. However, in animals, homologs have not been identified [48-50]. Unlike identified animal ion channels such as MEC-4/MEC-10, TRP or Piezo, MscL presents three novel features (1) cytoskeletal /ECM independent function, (2) nonselectivity (i.e., the channel is not ion specific and any molecule within the pore diameter limit can traverse the channel), and (3) large pore size [51-53]. Because of its role as an emergency release valve, bacterial null MS channel mutants indeed show markedly less viability under osmotic downshock [54]. When a bacterium is in a hypo-osmotic environment, osmosis across the cell's wall and membrane causes the bacterium to swell and stretches the membrane. As a response to the swelling, MscS and if needed, MscL, are activated allowing the cell to jettison

osmolytes (e.g., ions and small proteins) and rapidly equilibrate the inner and external cell osmolarity. Thus, MscL is meant to be triggered as a "last resort" and requires high energy to gate it. One of the major foreseeable limitations with the application of MscL is its high tension threshold of ~10 mN m^{-1}. As shown by previous patch-clamp experiments, the activation of MscL can require pressures close to the lytic tension of an unmodified bilayer [55, 56]. However, as discussed previously, single point mutations on the TM1 domain or addition of LPC lipid can greatly enhance MscL's mechanosensitivity.

Previous Work Involving MscL in Mammalian Cells: The application of MscL in mammalian cells was recently shown by Doerner *et al* [57]. In their work, they demonstrated functional expression of MscL WT and MscL G26C in CHO and HEK 293 cell lines using a lentiviral method. Despite performing patch clamp experiments with pressure driven gating of both MscL proteins in these mammalian cells, other mechanically driven gating was not demonstrated in the work. Instead, MscL gating and robust delivery of biomolecules ≤ 10,000 Da into live cells were shown through the treatment of the G26C mutant with 1mM MTSET reducing agent. Once membrane impermeable dyes such as phalloidin and AF-dextran were able to be delivered into live cells with reversible activation of the MscL G26C mutant. They found that continuous activation of MscL G26C for up to 8 minutes or more was cytotoxic. The addition of MscL and its chemically induced activation conferred the new and desirable property of efficient and non-cytotoxic delivery of small to large biomolecules into living cells.

However, a more detailed study on how MscL integrates into mammalian cells and its potential for conferring new mechanotransduction were not explored. In the following chapters of this thesis we detail research objectives aimed at utilizing MscL for the purpose of endowing novel, exogenous mechanotransduction in mammalian cells.

Research Objectives

We define mechanotransduction as a process consisting of cellular mechano-sensing, biochemical signaling, and changed cell function/behavior. To achieve novel mechanotransduction would then require generating new mechano-sensing, signaling, and/or mechanically driven function/behavior in cells. In the following three chapters, we will demonstrate how the functional expression of the *E. coli* MscL in mammalian cells endows the cells with new mechano-sensing capabilities such as the activation of MscL in the plasma membrane through membrane tension resulting from (1) osmotic down-shock and (2) new interactions with native mechano-sensory components, as well as altered cell function such as (3) impairment of cell migration in metastasis *in vivo* and narrow, 3D confinement *in vitro.*

Objective 1 - Activation of MscL as a Response to Osmotic Down-shock: As mentioned in *Chapter I*, previous work on MscL in mammalian cells did not explore MscL localization and mechano-sensing in detail[57]. We show that MscL localizes to multiple cellular membranes, including the plasma membrane. To then test MscL WT and G22S mutant mechano-sensing, we utilize osmotic down-shock. Based on

MscL's function as an emergency release valve in bacteria, we hypothesized that MscL could be activated in mammalian cells via membrane tension induced by osmotic down-shock. Working with larger mammalian cells, compared to bacteria, allowed for the use of fluorescent dye uptake as a reporter of MscL gating/activation. This mode of MscL activation was simple enough to be used as a functional assay in mammalian cells. Detailed experimental procedures and findings are provided in *Chapter II*.

Objective 2 - Activation of MscL via New Interactions with Native Mechanosensory Components: After showing expression and mechanical activation of MscL in mammalian cells we set out to investigate MscL gating as result of different types of mechanical perturbation, as shown in *Chapter III*. We were able to show robust activation of MscL via external force applied to surface integrins linked to intact actin cytoskeletons. These results showed a new interaction of MscL with native, mammalian mechano-sensory components. It is likely that direct perturbation of these mechano-sensors on the plasma membrane resulted in sufficient, localized membrane stress to activate adjacent MscL.

Objective 3 - Altered Cell Function: Migration: Lastly, in *Chapter IV* we investigated the effect of MscL mechanotransduction on the cell function of migration in cancer metastasis and then more specifically, 3D-confinements. During the physiological process of metastasis, cancer cells migrate through narrow pores and channels undergoing significant deformation[58, 59]; and in these 3D confined spaces cancer cells have been shown to utilize motility mechanism that rely on the actin-

cytoskeleton and myosin[60], or native aquaporins and ion channels[61]. We hypothesize that functional MscL expression in these metastatic cancer cells in these contexts would lead to MscL activation and impairment of cancer cell migration. Our findings in our *in vivo* mice model showed that there was a marked reduction in metastasis to the lung for MscL expressing cancer cells compared to controls. *In vitro* migration experiments using a biomimetic microfluidic device revealed that MscL activation due to 3D-confined migration could be responsible for the observed reduction in metastasis as a significant proportion of cancer cells with activated MscL could not migrate across a narrow, 3D channel of 30 μm^2 cross-section.

CHAPTER II

Functional Expression of Bacterial MscL in Mammalian Cells

The majority of this chapter is directly modified from Heureaux *et al.*, 2014 [62].

Introduction

The first major effort of this thesis was to show that bacterial MscL from *E. coli* can be expressed in mammalian cells, localize to the plasma membrane, and respond to membrane tension. Doerner *et al.* were the first to work with MscL in mammalian cells, but did not explore MscL localization and mechano-sensing in detail[57]. We worked with retinal pigment epithelial (RPE) cells to investigate this. Using adenovirus, we obtained efficient and tunable expression of MscL in RPE cells. Immunostaining showed that MscL localizes to multiple cellular membranes, including the plasma membrane. To then test MscL WT and G22S mutant mechano-sensing, we utilize osmotic down-shock. Based on MscL's function as an emergency release valve in bacteria[54], we hypothesized that MscL could be activated in mammalian cells via membrane tension induced by osmotic down-shock. Working with larger mammalian cells that are easily imaged on epi-fluorescence microscopes compared to bacteria, allowed for the use of fluorescent dye uptake as a reporter of

MscL gating/activation. This means of detecting MscL activation was simple enough to be used as a functional assay in mammalian cells.

Materials and Methods

Adenoviral MscL Expression System in RPE Cells: Constructs for the *E. coli* MscL WT as well as the gain of function mutant, MscL G22S were kindly provided by Boris Martinac (Victor Chang Cardiac Research Institute, Darlinghurst, Australia). The MscL constructs were sub-cloned into a tetracycline (tet) regulatable adenovirus vector using seamless cloning PCR [63]. His_6-tags were inserted at the N-termini of the MscL sequences for subsequent immunofluorescence imaging and Western Blot analysis. All constructs were verified by DNA sequencing at the University of Michigan DNA Sequencing Core. Adenovirus was generated and harvested from human embryonic kidney 293 (HEK293) cells transfected with the pADtet constructs [64]. Retinal pigment epithelial (RPE) cells were maintained in DMEM/F12 supplemented with 10% fetal bovine serum. To express MscL, RPE cells were co-infected with the adenoviruses containing MscL WT or MscL G22S (an MscL mutant with lower activation threshold) with encoded tet regulatable promoter and tetracycline transactivator (tTA) adenovirus with incubation duration of 8 –16 h prior to all experiments. Addition of tetracycline of various concentrations during infection incubation periods was used to verify proper function of the adenovirus expression system. For immunofluorescence imaging, infected RPE cells were fixed, permeabilized, and labeled with anti-His antibodies (Pierce Antibodies, Rockford, IL).

Quantitative analysis of infrared Western blots was conducted utilizing a LI-COR Odyssey Sa system (Lincoln, Nebraska USA).

Subcellular Fractionation of Cells: Cells from a 10-cm dish were lysed with 500 µl of subcellular fractionation buffer (250 mM sucrose, 20 mM HEPES (7.4), 10 mM KCl, 1.5 mM $MgCl_2$, 1 mM EDTA, 1 mM EGTA, 1 mM DTT, and 1 tablet of complete Protease Inhibitor Cocktail Tablets (Roche)), scraped and transferred to microcentrifuge tubes. The lysate was passed through a 25G needle 10 times and placed on ice for 20 minutes. To obtain the nuclear pellet, the tubes were centrifuged at 720 x g for 5 minutes and the supernatant was kept on ice. The nuclear pellet was washed 1X with the subcellular fractionation buffer. Supernatant from another 10-minute 10,000 x g spin from the previous supernatant was further separated by ultracentrifugation at 100,000 x g for 1 hour, leaving the cytosolic fraction in the supernatant, and the membrane fraction in the pellet. All samples were resuspended in SDS sample buffer and MscL expression was detected by Western blot using anti-His antibodies.

Osmotic Down-shock Experiments: RPE cells were infected with the adenoviruses encoding MscL for 16 hours prior the osmotic downshock experiments. Cells were incubated for a period of 2 minutes in saline solutions of different osmolarity with 10 mM HEPES and 100 µM propidium iodide (PI) (Sigma-Aldrich, St. Louis, MO) or 1 µg/ml Alexa Fluor 568 phalloidin (Life Technologies, Carlsbad, CA). PI and phalloidin are both impermeable to the plasma membrane and label the nucleic acids and the actin cytoskeleton respectively upon entering the cells. After

incubation, cells were washed with 1X phosphate buffered saline (PBS) twice and fixed with 4% paraformaldehyde. The nucleus was labeled with DAPI after cell permeabilization. PI intensity was quantified and normalized to total cell area in solutions at varying osmolarity. Imaging was performed on a Nikon TiE inverted microscope system, and image analysis was performed using ImageJ (http://rsb.info.nih.gov/ij/).

Results

Expression of Bacterial MscL in Mammalian Cells: We first sought to develop a viral-based strategy for introducing MscL into mammalian cells (Figure 2.1A). WT and mutant MscL constructs with N-terminal His_6-tag were cloned into a tetracycline-regulatable adenoviral vector. Infection with MscL-containing and tetracycline transactivator (tTA)-containing helper adenoviruses enables high expression efficiencies compared to transient transfection by using DNA vectors. Addition of tetracycline (tet) can tune the protein expression level by sequestering tTA. MscL expression in RPE cells infected with the adenoviruses containing MscL WT or MscL G22S exhibited a tetracycline dose dependent manner, as detected by both Western blot (Figure 2.1B), and immunofluorescence (Figure 2.1C). Nearly all the cells were infected and expressed MscL, and 50 ng/ml of tet was sufficient to turn off MscL expression. This experiment also served to validate our viral-based expression system for introducing MscL to mammalian cell lines. Since the His_6-tag is present on the cytoplasmic side of MscL, cells were permeabilized for

immunofluorescence examination. Interestingly, in addition to staining the plasma membrane, staining of MscL near the nucleus was also observed. To further confirm this observed localization of MscL, cell fractionation was performed and MscL was found in both plasma membrane and the nucleus (Figure 2.1D). It was not immediately clear whether MscL was inserted in the double lipid bilayer of the nuclear envelope or just to the outer lipid bilayer of the nucleus. Note that a direct comparison of the levels of expression cannot be made because the strong Western blot bands of MscL in the nuclear membrane was due to more concentrated fraction compared to the plasma membrane fraction.

Activation of MscL by Increasing Membrane Tension using Osmotic Shock: In E. coli, MscL and MscS subjected to an osmotic down-shock allows solutes to be released while maintaining cell viability. Cells with double null mutants are osmotically fragile[54]. Reconstitution of MscL into liposomes has demonstrated that MscL responds to membrane tension alone, and does not require any other proteins[21, 65]. To determine if MscL introduced in mammalian cells can be gated similarly by osmotic pressure, we first tested if hypo-osmotic solution could gate MscL with fluorescent phalloidin included in the medium. The large size of MscL's open pore allows free passage of large organic osmolytes. Phalloidin is ~800 Da and binds strongly to filamentous actin (F-actin) and not to monomeric actin. Furthermore, fluorescent phalloidin labels the F-actin strongly and is non-fluorescent when not bound to actin. Using this assay, we found that for RPE cells not expressing MscL, there was no phalloidin staining under both iso-osmotic and hypo-osmotic (10 mM

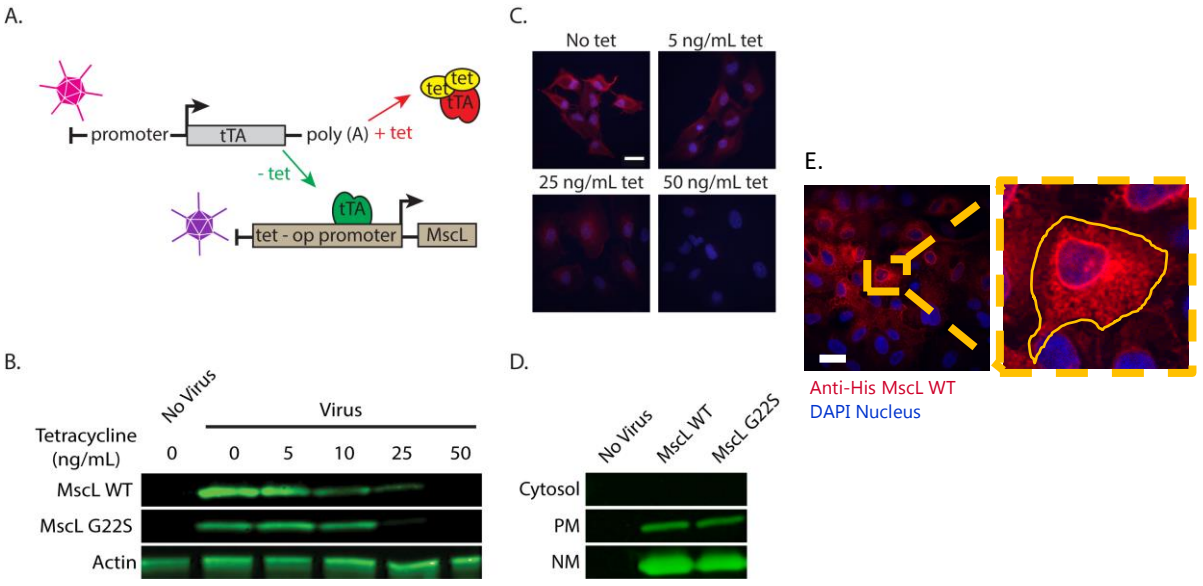

Figure 2.1 Viral Expression System for Mammalian Cells. (A) An adenovirus-based system for tetracycline-controlled transcriptional activation of MscL expression which consists of co-infection of tetracycline transactivator (tTA) and MscL viruses. In the absence of tet, tTA binds to the tet-op promoter upstream of the MscL gene and induces expression. In the presence of tet, tTA is sequestered, inhibiting expression of MscL. (B) Western blot analysis of infected whole cells and (C) fluorescent images of immunostained His-tagged MscL in mammalian cells cultured at different concentration of tetracycline. Scale bar = 25 μm. (D) Western blot analysis of fractionated cells showing MscL subcellular localization. (E) Confocal micrographs of immunostained His-tagged MscL in RPE cells. Scale bar = 25 μm

HEPES) conditions, as expected (Figure 2.2A). In RPE cells with expressed MscL, strong phalloidin staining was observed in cells that were under hypo-osmotic condition but not in iso-osmotic condition. Together, these results confirmed the functional expression of MscL in RPE cells. As a non-selective channel that molecules up to 6.5 kDa in size can permeate through, other osmolytes can also transit through the opened MscL [66].

To further investigate the responsiveness of MscL activation by osmotic pressure, we used PI, an intercalating fluorescent molecule when bound to nucleic acid after entering the cells, to determine the threshold of MscL activation. Some dye uptake was evident at 100 mOsm and the influx continued to increase with

decreasing solution osmolarity. As expected and consistent with the earlier result, no PI uptake was detected at any osmolarity when RPE cells did not express MscL (Figure 2.2B, C). At the low end of the osmolarity, cells expressing MscL G22S took up significantly more PI than MscL WT cells. Interestingly, it appeared that MscL WT had a more dye uptake or more activation than MscL G22S. In addition, since MscL was found to localize to the nuclear membrane as well, we asked whether osmotic down-shock would affect the nucleus. Since PI binds strongly to nucleic acid, presence of PI labeling in the nucleus does not necessarily indicate that MscL is functioning in the nuclear membrane. Under iso-osmotic conditions, nuclei sizes were similar between control cells and cells expressing MscL. The nuclei of MscL expressing cells were smaller under hypo-osmotic conditions for both WT and G22S mutant (Figure 2.2D), suggesting that MscL could be activated on nuclear membrane as well. The increase in osmotic pressure in hypo-osmotic solution arises from the tendency of water to cross the cell membrane, which increases cell volume, and thereby membrane tension.

Osmotic down-shock experiments were also performed on Chinese Hamster Ovary (CHO) cells expressing MscL WT and G26C cells (courtesy of Doerner *et al.* [57]) (Figure 2.2E) and compared to MTSET activation. The CHO MscL WT cells showed higher PI uptake for 175 mOsm and 10 mOsm than CHO MscL G26C cells indicating that MscL WT is more mechanosensitive than MscL G26C in CHO cells. CHO MscL G26C cells showed robust uptake of PI when chemically activated with 1mM MTSET in media for 8 minutes while MscL WT cells showed no uptake.

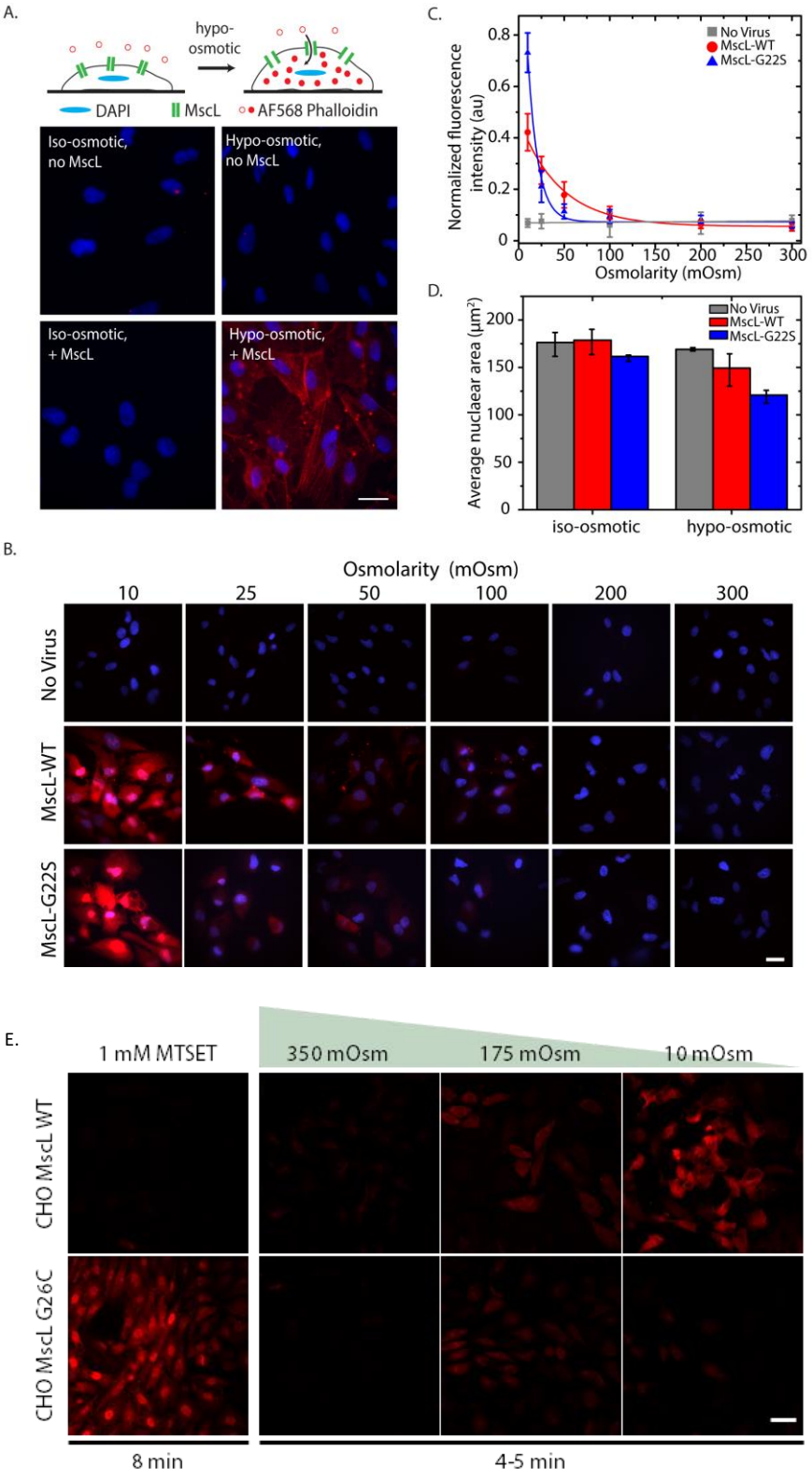

Figure 2.2 Osmotic Down-shock Experiments on MscL Expressing RPE and CHO cells. (A) Cartoon description of osmotic shock assay (top). Under hypo-osmotic conditions, mammalian cell membranes swell leading to increased

membrane tension and MscL activation, which allows for uptake of fluorescent phalloidin. Fluorescent images of fixed, MscL WT infected and non-infected cells incubated under iso-osmotic and hypo-osmotic solution containing fluorescent phalloidin for 8 minutes (bottom). F-actin labeling is shown in red and DAPI labeling in blue. (B) Fluorescent images showing PI (red) uptake in cells expressing MscL WT and G22S and in non-infected cells. (C) Average PI uptake after two minutes incubation with PI solutions of decreasing osmolarity (n=3, n_{cell} per condition is ~100). (D) Average nucleus area of non-infected cells and those expressing MscL WT and G22S in iso-osmotic and hypo-osmotic conditions (n=3, n_{cells} = ~100). Error bars are standard error of the mean. (E) Fluorescent images showing PI uptake of MTSET condition and osmotic down-shock performed on CHO cells expressing MscL WT and MscL G26C. Scale bars = 25 μm.

Discussion

Our finding that MscL was localized to nuclear membrane of the infected RPE cells, in addition to the plasma membrane, and presumably also to other cellular compartments, is interesting. This may not be entirely surprising given that MscL does not have a leader sequence targeting it to the plasma membrane. Thus, it may be able to insert into any cellular membranes as it readily inserts into liposome bilayers, and leading to interesting consequences. For example, expression of MscL in mammalian cells was found in this study to be responsible for the influx of small molecules such as PI and phalloidin during an osmotic down-shock. Remarkably, osmotic down-shock also decreased nuclei sizes. The precise mechanism of how this occurred is unclear, but the possibility that MscL could potentially alter the mechanics of the nucleus is intriguing and further studies are required to determine if nuclear functions are affected by MscL activation from osmotic downshock. In cells expressing MscL G22S, significantly higher PI uptake was observed with the strongest osmotic down-shock tested compared to MscL WT, but more uptake was observed for MscL WT than MscL G22S for the other, less extreme hypo-osmotic conditions. Potentially, there could be differences in the activation of the two MscL molecules that resulted in different opening states such as channel kinetics, and/or

sub-conducting states and thresholds. A possible mechanism is the differences between the closed expanded state and the tendency for GOF mutants to prefer lower sub-conducting states until triggered by a higher tension range [27]. Though this was not previously observed for MscL G22S mutant specifically, it has been observed in other gain of function mutants, and there is still a possibility that this can be true in our mammalian cell system. Given that MscL G22S is more sensitive to tension, it may silently expand sooner than WT MscL, which in turn would relax membrane tension due to the low osmolarity. This would result in MscL G22S appearing to open at a higher tension/lower osmolarity threshold than MscL WT. MscL G22S also exhibits flickering kinetics (i.e., dwell times ~2 ms) that can also result in a reduction in uptake.

The results from the osmotic down-shock experiment on CHO cells expressing MscL WT and G26C appear to be in direct contrast with what has been found previously in spheroplasts where MscL G26C had a tension threshold ~0.76x of MscL WT making it a gain of function mutant [67]. However, MscL G26C channel kinetics under tension activation is < 1 ms and MscL WT kinetics vary from < 1 ms to 30 ms. The MscL G26C flickering kinetics can result in a reduction in the amount of dye that can pass through the channel similar to what was observed with MscL G22S.

Conclusions and Implications

In summary, we were able to show successful expression of MscL in RPE cells and MscL localization to multiple cellular membranes including the plasma

membrane. MscL mechano-sensing was retained and the channel could be activated by osmotic down-shock. For our experiments, we used visualization of dye uptake as an indicator of MscL activation and we found that dye uptake correlated to the extent of osmotic shock. Finally, we found that MscL activity is increased with the G22S mutant for more extreme shock (e.g., ~10 mOsm in our experiments).

Our findings have already led to impactful implications. The method of osmotic down-shock was simple and robust enough to be used as a functional assay of MscL in mammalian cells. Using dye uptake as a qualitative reporter of MscL activation in mammalian cells is more accessible than traditional means such as patch-clamp electrophysiology. Importantly, we show that osmotic shock activation of MscL can be used to deliver large and impermeable molecules into living cells, which can be used as a tool for many scientific applications not exclusive to the field of mechanobiology.

Activation of MscL via osmotic down-shock now leads us into investigating activation of MscL in mammalian cells via other types of mechanical perturbation. By doing so, we can expand MscL's mechano-sensing repertoire for mammalian cells and widen its applicability in mechanobiology.

CHAPTER III

Activation of MscL in Mammalian Cells via Different Modes of Mechanical Perturbation and Linking MscL Activity to the Cytoskeleton

The majority of this chapter is directly modified from Heureaux *et al.*, 2014 [62].

Introduction

The importance of cytoskeleton for activating endogenous mammalian MS channels has been suggested by many studies [68-70]. This is in contrast to bacterial MS channels that do not require the bacterial cytoskeleton to function. Although neither MscL nor MscS homologues have been identified in animal and human cells to date, reconstitution of functional MscL activity in mammalian cells was recently demonstrated [57]. This revealed that MscL mechanical activation via pressure modulated patch clamp is possible and molecular transport can be achieved by charge-induced activation of mutant MscL G26C. Even though there is a well-accepted mechanism for MscL activation by membrane tension in bacteria, whether and how MscL can be opened by other modes of force transduction in mammalian cells were not investigated. The ability to express MscL in mammalian cells presents new opportunities for studying the activation mechanism of MscL and potentially can introduce new mechanostransduction pathways to mammalian cells. In this study, we examined MscL function under different mechanical perturbations in mammalian cells. We performed micropipette aspiration of single cells and fluid shear stress

experiments to characterize these channels in RPE, mammalian cells. Both methods failed to gate MscL under our experimental conditions. Interestingly, using a relatively new technique, acoustic tweezing cytometry (ATC) [71], where acoustic excitation of lipid-coated microbubbles targeted to the cell membrane via integrin receptors, robustly gated MscL and the ATC-mediated activation was dependent on an intact cytoskeleton and the coupling to integrin receptors. Our results demonstrate that the activation of a bacterial MS channel expressed in mammalian cells can be mediated through localized membrane stress that is dependent on the actin cytoskeleton.

Materials and Methods

Adenoviral MscL Expression System in RPE Cells: Refer to Chapter II.

Micropipette Aspiration: Aspiration was applied by a homebuilt micropipette aspiration system with a graduated manometer and an in-line DP15 pressure sensor (Validyne Engineering, Northridge, CA). Shortly before aspiration, RPE cells expressing MscL or not were lifted by incubation with citric saline. The cells were spun down and resuspended in culture medium. The suspension and 50 μM PI were then added to a custom viewing chamber. Glass micropipettes with inner diameters of 5 μm were filled with 0.2% bovine serum albumin (BSA) in PBS in order to allow smooth movement of cell membrane inside the pipette. Negative pressure in the micropipette tip was generated by aspirating water from the main manometer reservoir and increased gradually in 100 Pa increments. Sudden pressure shock was

applied to aspirated cells by manually tapping the tubing attached to the micropipette. Nikon Advanced Modulation Contrast optics (NAMC) mounted on a Nikon Ti-S microscope and CoolSnap MYO CCD camera (Photometrics, Tucson, AZ) were used to acquire live-cell bright-field and fluorescent images.

Shear Flow Experiments Cells: were seeded in μ-slide VI0.1 microfluidic channels (ibidi, Verona, WI) overnight prior to infection with MscL adenoviruses. A 60-mL plastic syringe containing 50 μM propidium idodide in DMEM/F12 medium was mounted to a HA PhD Ultra syringe pump (Harvard Apparatus, Holliston, MA) and connected to the microchannels using sterilized Tygon tubing and Luer fittings. Shear stress in the channels was controlled by varying the flow rate. The shear stress, τ (in dyne/cm^2), as a function of volumetric flow rate, Q (in μl/min), is $\tau = 0.1067Q$ for a fluid viscosity of 0.01 dyne/cm^2 (per manufacturer's application note). Each channel was exposed to a fluid shear stress for 4-5 minutes. Live cell microscopy was performed on the Nikon Ti-E inverted fluorescence microscope equipped with sCMOS camera (Hamamatsu Photonics) and controlled via μManager software (http://www.micro manager.org).

Acoustic Tweezing Cytometry (ATC) Experiments: A similar ATC setup described previously was used in this study [71]. One day prior to ATC, RPE WT cells were seeded on glass bottom culture dishes (MatTek Corporation, Ashland, MA) coated with 50 μg/mL fibronectin from human plasma (Sigma-Aldrich, St. Louis, MO). Right before ATC experiments, Targesphere™-SA microbubbles (Targeson, San Diego, CA, USA) were mixed with biotinylated Arg-Gly-Asp (RGD) peptides (Peptides

International, Louisville, KY, USA) for 20 min at room temperature, with a volume ratio of 5:1 of microbubbles ($5x10^8$ mL^{-1}) to RGD (0.01 mg/mL). To attach the microbubbles to cells, the culture media from the cell-seeded 35 mm glass bottom dish was removed followed by immediate addition of 20 µL of microbubble-RGD mixture.

The small fluid volume permitted inversion of the culture dish to allow microbubbles to float upward to facilitate attachment of the microbubbles to the cells via RGD-integrin bindings. After 10 min, the dish was flipped back and unbound microbubbles were removed by a gentle wash with culture media. During experiments, the cell-seeded dish was placed on a 37°C heating stage on an inverted microscope (Eclipse Ti-U; Nikon, Melville, NY, USA). A 40× objective (0.75 NA; Nikon, Melville, NY, USA) was used for observation of cells and microbubble activities. A 10 MHz focused transducer (Olympus, Waltham, MA, USA) was positioned at an incident angle of 45° to apply ultrasound pulses to excite the microbubbles attached to the cells. The transducer was driven by a waveform generator (Agilent Technologies 33250A, Palo Alto, CA) and a 75 W power amplifier (Amplifier Research 75A250, Souderton, PA). The ultrasound pulses applied in this study each had a fixed pulse duration (PD) of 50 ms and pulse repetition frequency (PRF) was 5 Hz. The total duration of ultrasound application was 10 s with the acoustic pressure amplitude of the ultrasound pulses as a variable. The free field acoustic pressure was measured using a 40 µm calibrated needle hydrophone (Precision Acoustics HPM04/1, UK). The application of ultrasound was synchronized with a high-speed camera (Photron FASTCAM SA1, San Diego, CA), which was used

to capture the ultrasound-driven microbubble activities at a frame rate of 5,000 frames/s. The translational displacement and the radius of the microbubbles before, during, and after ultrasound application were obtained from the high-speed image sequences using a custom MATLAB program. Only cells with bound microbubbles that had visible movements during ultrasound pulses were included in our quantitative analysis.

Results

Micropipette Aspiration of MscL Expressing RPE Cells: To see if cortical tension alone, without the concomitant increase in cell volume (like that observed during the osmotic down-shock experiments), could activate MscL, we utilized micropipette aspiration to manipulate cortical tension of RPE cells in suspension. The suction pressure is typically small relative to the osmotic pressure of the isotonic media, so the cell will deform without an apparent increase in volume. Here, micropipettes with inner diameters of 5 μm were used on RPE cells which have an average apparent diameter of 15 μm. Our custom micropipette aspiration setup was able to apply aspiration pressures of up to ~ 1 kPa. By including PI in the external medium, activation of MscL by micropipette aspiration was tested (Figure 3.1A). We did not observe PI uptake into both MscL WT and G22S cells for the full range of our aspiration pressure (Figure 3.1B). However, when a sudden change in pressure was introduced by gently tapping the tubing connecting to the pipette, PI uptake was observed for every condition, including cells without MscL, suggesting that the

sudden pressure shock may have led to transient membrane disruption. To contrast the previous osmotic down-shock experiments, a spread RPE cell can easily cover > 1500 μm^2 area, suspended RPE cells may have significant amount of membrane reservoirs within the membrane folds. Thus, the aspiration pressure applied may not be able to significantly increase cortical tension, as one would initially expect.

Shear Stress by Fluid Flow: Mechanochemical signal transduction by shear-sensitive mechanoreceptor allows sensing of hemodynamic forces, particularly in endothelial cells [72]. We next asked whether shear stress could possibly activate MscL in mammalian cells. Shear stress can be controlled using microfluidic channels with well-defined geometry (Figure 3.2A). While the cultured cells in microchannels expressed MscL successfully (Figure 3.2B), no robust MscL activation was detected in cells subjected to shear stress up to 400 dyne/cm^2 (Figure 3.2C). At 400 dyne/cm^2 of shear stress, a few cells expressing MscL G22S were observed with PI uptake, but cell detachment was evident when shear stress above 400 dyne/cm^2 was applied, as others have shown [73]. As a positive control, MscL expressing cells in microfluidic channels took up PI when subjected to an osmotic down-shock (Figure 3.2D). Because the fluidity of the lipid bilayer membrane, flow-generated shear stress is unable to exert forces directly to the lipid molecules to induce membrane tension.

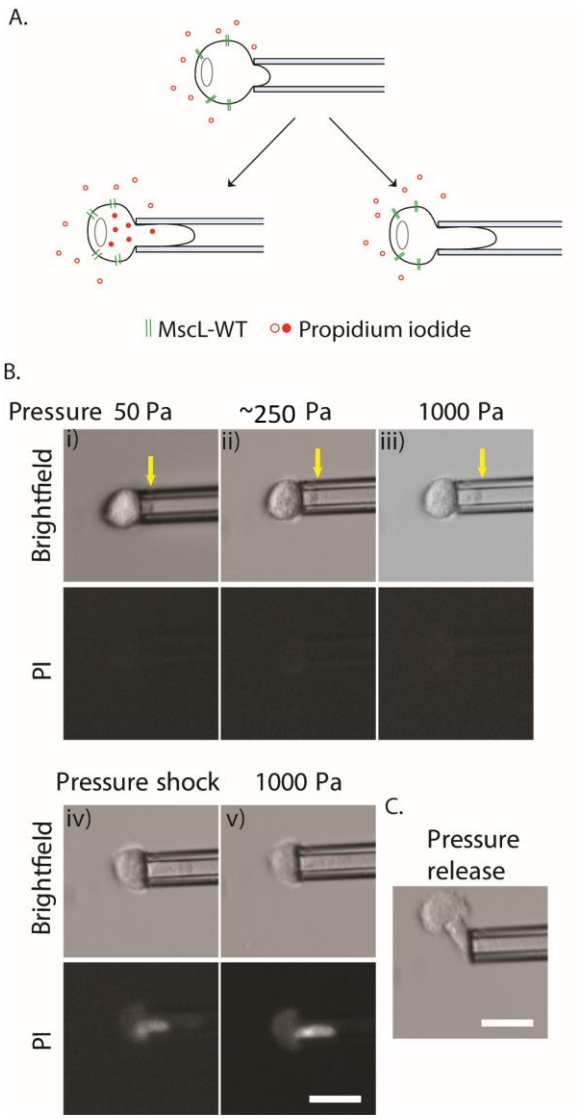

Figure 3.1 Micropipette Aspiration. (A) Cartoon of micropipette aspiration on MscL expressing mammalian cells. (B) Brightfield and corresponding fluorescent images showing PI uptake for a MscL WT expressing cell as applied aspiration pressure is increased (i – iii). The edge of the cell protrusion drawn into the micropipette is indicated by yellow arrows. Pressure shock is applied to the cell when the tubing directly connected to the micropipette is manually tapped (iv-v). (C) Aspiration pressure is released. Scale bars = 15 μm, $n_{cell} > 8$.

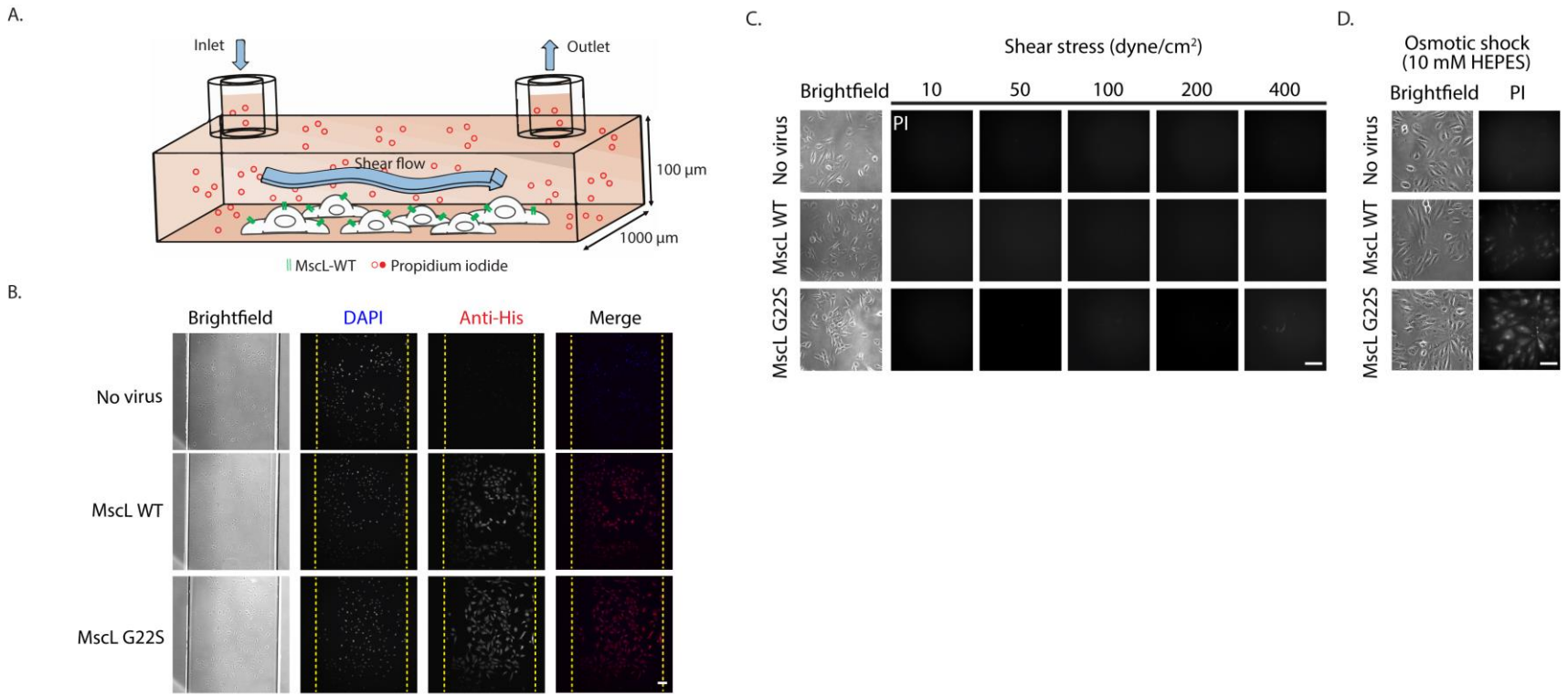

Figure 3.2 Flow Induced Shear Stress for Activation of MscL in Mammalian Cells in Microfluidic Channels. (A) Cartoon showing shear flow of medium containing PI on MscL infected cells seeded in microfluidic channels. (B) Bright-field and immunofluorescent images of non-infected, MscL WT, and MscL G22S infected cells in microfluidic channels. DAPI and anti-His were used to stain for the cell nucleus and His-tagged MscL respectively. Scale bar = 100 µm. (C) Bright-field and fluorescent images showing PI uptake for no virus, MscL WT, and MscL G22S infected cells subjected to different shear stresses for 4 – 5 minutes in microfluidic channels. (D) Bright-field and fluorescent images showing PI uptake for no virus, MscL WT, and MscL G22S infected cells incubated in PI-containing hypo-osmotic solution for 2-4 minutes in microfluidic channels. Scale bars = 25 µm for (C) and (D).

Acoustic Tweezing Cytometry and Direct Linkage to the Mammalian Cell Cytoskeleton: Shear deformation becomes relevant if the membrane is coupled to structures such as the cytoskeleton. To test if localized stress to the cells could potentially induce activation of MscL expressed in mammalian cells, we conducted a series of experiments using acoustic tweezing cytometry (ATC) (Figure 3.3A). ATC uses ultrasound pulses to excite gas-filled microbubbles that were functionalized with Arg-Gly-Asp (RGD) peptide and attached to integrin receptors of the cells via the robust interaction of ultrasound with the integrin-anchored microbubbles [24]. Ultrasound pulses generate a directional force, the acoustic radiation force [74], on the microbubbles, and the displacement of the integrin-anchored microbubbles from their original location leads to targeted stress to the cells through the microbubble-integrin cytoskeleton linkage. In addition, ultrasound application readily generates cavitation of the microbubbles (rapid volume expansion and contraction), which induced microstreaming of fluid, thus shear stress, near the microbubbles [75]. Our previous work has shown that ATC using ultrasonic excitation of RGD-functionalized microbubbles bound to integrins elicited strong cytoskeleton contractile response that required an intact actin cytoskeleton and Rho/ROCK signaling [71]. In this study, functionalized microbubbles were introduced to cells seeded on a glass bottomed culture dish such that 3.7 ± 2.2 (n = 40 cells) microbubbles were attached to each of the cells (Figure 3.3B). Using a 10 MHz transducer mounted at a 45^{o} angle, microbubbles were subjected to 10 s of application of ultrasound pulses with a duty cycle of 25% and pulse repetition frequency of 5 Hz. These parameters minimized the

cavitation effect compared to the directional force (acoustic radiation force) exerted on the microbubbles. The primary acoustic radiation force was generated by the incident ultrasound field on a microbubble via momentum transfer, and can be calculated as $F = \frac{2\pi P_A^2 R_0}{\rho_0 c\omega} \frac{\delta_{tot}\omega_0/\omega}{(((\omega_0/\omega)^2-1)^2+(\delta_{tot}\omega_0/\omega)^2)}$ [74], where P_A is the acoustic pressure amplitude, R_0 is the equilibrium radius of microbubble, δ_{tot} is the total damping constant (0.1), ρ_0 is the medium density (1000 kg/m^3), and c is the speed of sound in medium (1500 m/s), $\omega_0 = 2\ \pi f_0$, where f_0 is the resonance frequency (3.5 MHz) of the lipid coated microbubble with a radius of 2 μm [76], and ω is the frequency of the ultrasound applied (10 MHz).

Using a pressure amplitude between 0.047 MPa and 0.095 MPa, a force between 15 pN and 60 pN can be generated on a microbubble (Figure 3.4). Large amplitude expansion/contraction of microbubbles (strong cavitation), which typically occurs under high acoustic pressures or when the frequency of the incident ultrasound field is close to the resonant frequency of the microbubbles, can lead to transient membrane disruption by sonoporation that permits transport of exogenous molecules [77]. Large amplitude cavitation often leads to reduction in microbubble size over time, due to gas leakage from the disrupted protective lipid layer of the encapsulated microbubbles. To ensure cavitation was not the cause for PI uptake by disrupting the cell membrane in our experimental study, we employed relatively low acoustic pressure amplitudes and 10 MHz center frequency, which was far away from the microbubble resonant frequency. High-speed imaging observation confirmed that microbubble expansion and contraction was minimal (< 5% of the equilibrium radius)

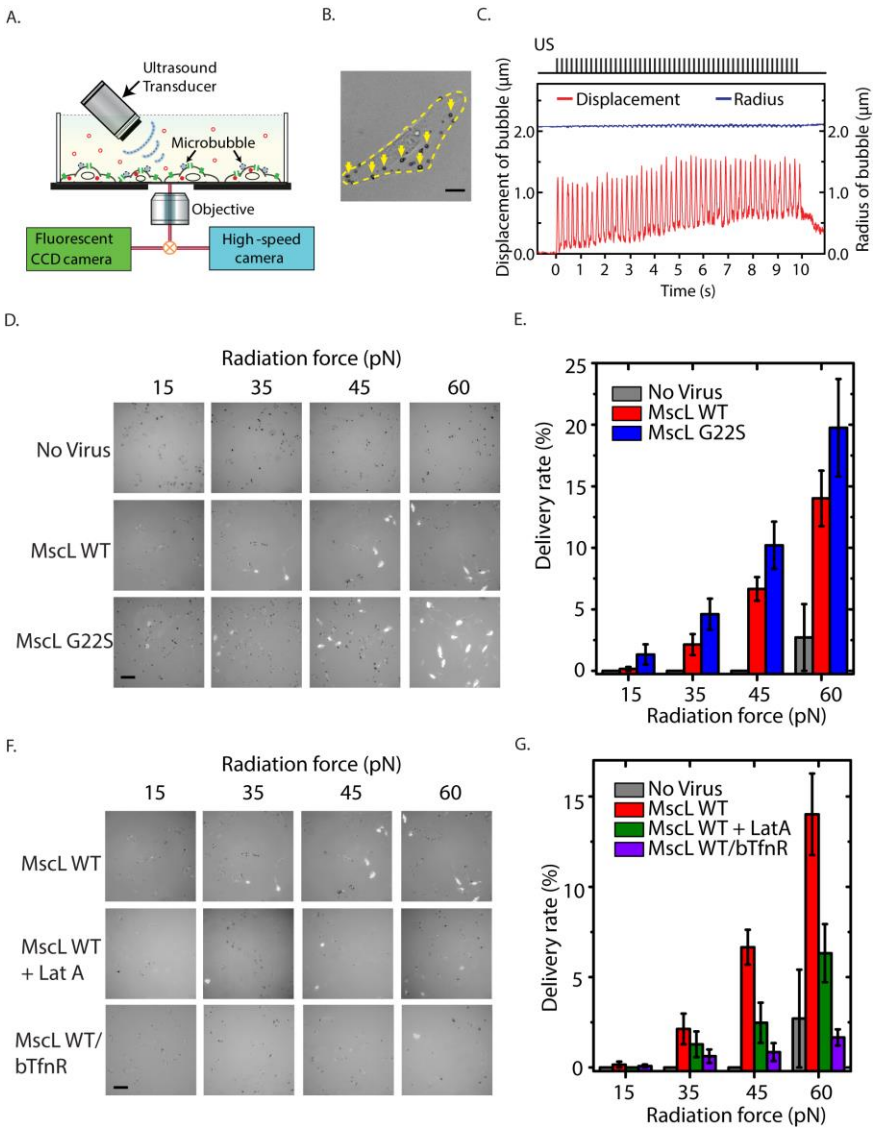

Figure 3.3 Acoustic Tweezing Cytometery for Activation of MscL in Mammalian Cells and Uptake of Impermeable Molecules. (A) Experimental setup of ultrasound excitation of targeted microbubbles attached to the membrane of cells (drawing not to scale). (B) Brightfield image of an RPE cell outlined in yellow witch RGD functionalized microbubbles attached indicated by yellow arrows. (C) Ultrasound- (US) induced microbubble activities. Typical translational displacement and radius profile of a microbubble during the 10-second US stimulation (pulse duration = 50 ms, pulse repetition frequency (PRF) = 5 Hz, Acoustic pressure = 0.071 MPa). (D) Fluorescent images of MscL WT, MscL G22S, and non-infected cells with RGD-microbubbles subjected to different radiation forces. Cells with PI uptake after US application exhibit bright fluorescence. (E) Delivery rate (percentage of cells with PI uptake after US application) of MscL WT, MscL G22S, and non-infected cells with integrin-bound, RGD-microbubbles (n = 3 - 5, n_{cell} = 100 - 400). (F) Fluorescent images showing PI uptake after US application for MscL WT infected cells not treated and treated with 50 nM latrunculin A with RGD-microbubbles, and cells infected with MscL WT and bTfnR adenoviruses with avidin functionalized microbubbles bound to biotinylated-transferrin receptors. (E) Delivery rate for MscL WT infected cells not treated and treated with 50 nM latrunculin A with with integrin-bound microbubbles and MscL\bTfnR infected cells with biotinylated-transferrin receptor-bound microbubbles (n = 3, n_{cell} = ~100 - 300). Scale bars = 25 μm for (B), (D), and (F). One-tailed t-test comparing MscL-expressing vs. non-infected cells showed significant differences between all conditions ($p < 0.05$), except for 15 pN. Error bars are standard error of the mean.

and the size of microbubbles remained stable throughout ultrasound application (Figure 3.3C). Furthermore, experiments with PI in the medium showed no uptake in the control cells (without MscL), with or without microbubbles, indicating no cell membrane disruption by ultrasound application. Translational displacement of the microbubbles was observed with an average displacement of ~ 1 μm achieved during each ultrasound pulse. During the pulse-off period, the microbubbles partially returned to their original positions, dictated by the elastic properties of the microbubble-focal adhesion-cytoskeleton linkages.

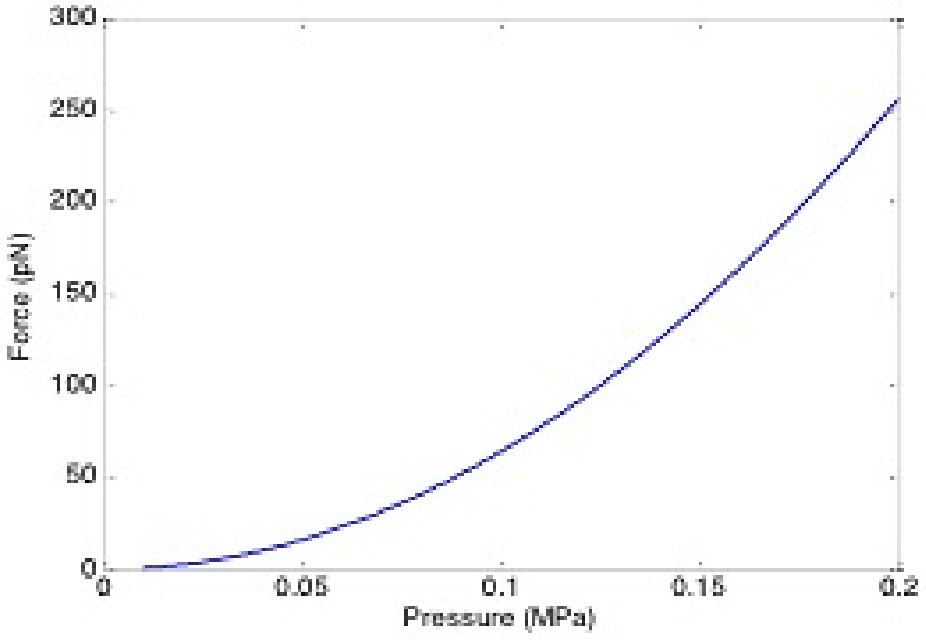

Figure 3.4 Radiation Force Applied to Microbubbles. Shown as a function of ultrasound pressure produced by the 10 MHz transducer for the ATC system used.

The creep in the displacements may be due to the short time interval between pulses such that there may not be enough time for a full recovery of microbubble displacements. Interestingly, with application of ATC to apply forces to the integrin

receptors, cells expressing MscL clearly took up PI as the acoustic radiation force increased from 0 to 60 pN, in contrast to uninfected cells without visible PI uptake (Figure 3.3D), indicating gating of the MscL expressed in the cells by ATC stimulation. The percentage of cells that took up PI increased to up to about 20%, and MscL G22S expressing cells had a higher percentage of cells with PI uptake compared to MscL WT cells (about 14%), consistent with the lower tension threshold for MscL G22S expressing cells (Figure 3.3E). To exclude the possibility that virus-infection of cells somehow caused the cells to become more sensitive to ATC perturbation, we tested whether RPE cells expressing adenovirus-encoded biotinylated transferrin receptor (bTfnR) using a site-specific labeling approach developed previously [78] took up PI when subjected to ATC stimulation. We found that bTfnR expressing RPE cells did not take up PI at any applied forces by ATC, indicating that the viral infection had no effect on PI uptake. As RGD-bound microbubbles were targeted to integrin receptors, we tested whether MscL activation could occur by forces applied to other membrane receptors such as bTfnR. With microbubbles bound to cells expressing both bTfnR and MscL, we found no PI uptake in these cells subjected to the same ATC stimulation (Figure 3.3F), suggesting that force transduction through the integrin-focal adhesion complex is critical for the observed activation of MscL and PI uptake by ATC stimulation. Consistently, mild disruption of the actin cytoskeleton by treating the cells with 50 nM of latrunculin A, an actin monomer binding drug, reduced the PI delivery rate significantly (Figure 3.3G). Together, these results showed that the observed activation of MscL is mediated through localized

mechanical stress induced by ultrasound actuation of integrin-anchored microbubbles on the cells via the microbubble-integrin-cytoskeleton linkage in an actin dependent manner.

Discussion

Mechanosensation is one of the most ubiquitous phenomena in living systems and MS channels constitute the simplest mechanism of mechanotransduction [79]. However, our understanding of MS channels is far from complete. Studies of mechanosensation in bacteria have led to the discovery of MS channels that gate by lipid bilayer tension, while identification of the gating mechanisms of MS channels in eukaryotes has been much more challenging due to the rarity of certain sensory cells and the difficulty in assaying the function of candidate mechanotransudction molecules[80]. Our results presented in this study identified a new activation mechanism for gating MscL in a different cellular context, by employing a new cellular mechanics tool (ATC) and on mammalian cells expressing bacterial MscL.

Our current study using micropipette aspiration setup indicated that up to ~1 kPa of aspiration pressure was insufficient to activate MscL in RPE cells. We found that the RPE cells behaved more like an elastic solid than a liquid droplet as it was possible to apply aspiration pressures to have $L_p / R_p > 1$ in our experiments, where L_p is the aspiration length and R_p is the micropipette radius, without causing the cell to be completely aspirated into the micropipette. The equivalent cortical tension for solid cells at the point $L_p / R_p = 1$ is ~ $2.2 ER_p$ [81], where E is the Young's modulus. Using

E as 500 pN/μm^2 and R_p of 5 μm, the cortical tension is 5.5 mN/m. This tension is about half of the membrane tension of ~10-12 mN/m reported to gate MscL when reconstituted in liposome [82, 83]. However, since our suction pressure was an order of magnitude smaller than what was found to gate MscL in mammalian cells, ~13 kPa in CHO or HEK cells [57], we believe the cortical tension did not increase significantly past the point L_p / R_p = 1 in our experiments. This could be due to a significant membrane reservoir of the RPE cells in suspension that buffered changes to increasing suction pressure. Additional studies are needed to determine exactly the cortical tensions generated in the RPE cells during micropipette aspiration to obtain better understanding of the gating threshold of MscL in these cells.

Our experiments also showed that MscL in RPE cells was not sensitive to flow-induced shear stress up to 400 dyne/cm^2. At 400 dyne/cm^2, a surface tension of up to 0.1 mN/m could be induced for a 25 μm cell, which was much lower than the reported ~12 mN/m for MscL activation [83]. Thus, the inability for shear stress to open MscL in our experiment may be primarily due to the insufficient membrane tension to gate MscL that is produced by fluid flow. Increasing the flow velocity to increase shear stress was not feasible in our experiments due to cell detachment, indicating the limitation of the use of flow-induced shear stress as a robust mechanism for gating of MscL expressed in RPE cells. As such, shear-sensitive MS channels could have a very different gating mechanism than sensing pure membrane tension as the primary stimulus. For example, tethering to the cytoskeleton may be important in the activation mechanism for shear-sensitive MS channels. MS channels gating is

employed in hair cells and neuronal cells which have a direct connection between the channels and the cytoskeleton and/or extracellular matrix (ECM) in order to confer directional sensitivity [80, 84]. Furthermore, a recent work postulates that stiffened lipid platforms that can direct, rescale, and confine force may be a plausible mechanism that is used by mammalian cells [85]. This is an interesting possibility because cell membranes are highly heterogeneous and cells have extensive cytoskeleton networks that connect to the ECM through transmembrane integrin receptors. Since cytoskeleton membrane interaction plays a key role in regulating membrane properties, cytoskeleton and ECM may serve to modulate the dynamic range in gating of MS channels [86]. The use of the novel ATC technique for applying mechanical forces provided the opportunity to investigate the involvement of this mechanism in MscL gating. Our finding that local force application using ATC could open MscL in an actin-dependent and integrin-dependent manner supports this idea, and is consistent with a previous study that showed direct mechanical stimulation of actin stress fibers activates MS channels in endothelial cells [68],where a stretching force of 5.5 pN exerted on stress fibers resulted in inward current from MS channels [68]. In this study and indicated by previous work, ATC applied local mechanical stresses to the cells via acoustic actuation of integrin-bound microbubbles. Although the detailed process of force generation on the cells is the focus of on-going investigations, it is clear that the displacements of the integrin-bound microbubbles by the acoustic radiation force are involved in the stress exerted to the cells. On the other hand, fluid microstreaming induced by a cavitating microbubble during

ultrasound application can also exert localized shear stress on the nearby cells, as demonstrated previously [75]. However, in this study, the use of low acoustic pressures and center frequency of 10 MHz likely reduced the impact of cavitation relative to microbubble displacement. While the force that we applied to the microbubbles corresponding to activation of MscL ranged from 30 – 60 pN, how this force is translated to the cells to contribute to gating MscL requires further investigation. In addition, the effects of the number of microbubbles and duration of ATC stimulation will need to be elucidated. Nonetheless, the forces we applied to cells by the use of ATC to open MscL is likely greater than the 0.5 pN force that is exerted by a globally applied shear stress of 400 dyne/cm^2, assuming a protein of 5 nm in diameter. More importantly, we believe it is the localized force transduction via the microbubble-integrin-actin cytoskeleton that was critical for the gating of MscL. The finding that exerting the same force using ATC on microbubbles targeted to TfnR did not gate MscL supports the idea that force transduction via integrin actin cytoskeleton is responsible for the observed MscL gating. Interestingly, there are no known molecular interactions between MscL and any mammalian cellular components, thus force transduction via cytoskeleton is highly unlikely to act through a direct tethering mechanism that has been proposed to pre-stress MS channels and affects their sensitivity [87].

Instead, we believe that a local change in membrane tension was generated by ATC and gated MscL in our experiments, revealing a new mechanism for gating MscL in mammalian cells. Our ATC experiment also provides the first demonstration

where delivery of molecules across the cell membrane can be achieved through the activation of a non-specific MS channel without transient membrane disruption through sonoporation, providing an intriguing mechanism for intracellular molecular delivery. The use of ultrasound in ATC is advantageous as it can exert forces on multiple cells at the same time via biocompatible and multifunctional microbubbles in both 2D or 3D settings with a force range that is compatible with biological studies. Our results reported in this study demonstrate a new platform for further investigating MscL gating under different cellular conditions. The ability to functionally express MscL in mammalian cells could provide new opportunities for mechanobiology studies. MscL expression in non-mechanosensitive cells can render them mechanosensitive and be used as a novel mechanism for molecular delivery in these cells. A number of diseases such as muscular dystrophy, sickle cell anemia, and cardiac arrhythmias have been linked to defects in activating MS channels. Thus, it is tantalizing to suggest that engineered MscL with precise gating behaviors could be used as a therapeutic tool. Finally, one could also imagine the potential of using MscL in building functional cellular devices that are mechanosensitive. mechanism for gating MscL in mammalian cells. Finally, one could also imagine the potential of using MscL in building functional cellular devices that are mechanosensitive.

Conclusions and Implications

In summary, we were unable to robustly activate MscL in RPE cells using shear flow on adherent cells and micropipette aspiration likely due to insufficient

membrane tension. However, ATC on RPE cells expressing MscL WT and G22S resulted in MscL activation where MscL G22S was more responsive to ATC. Activation was contingent on (1) microbubbles being bound to integrins (i.e., integrins were directly perturbed) and (2) an intact actin cytoskeleton.

Here we show how MscL and ATC can be used to deliver impermeable molecules into living cells without the need for bubble cavitation. Importantly we postulate a model for native integrin-actin cytoskeleton and MscL interaction where direct perturbation of actin-linked integrins can result in enough localized membrane force to activate MscL in mammalian cells (Figure 3.5)

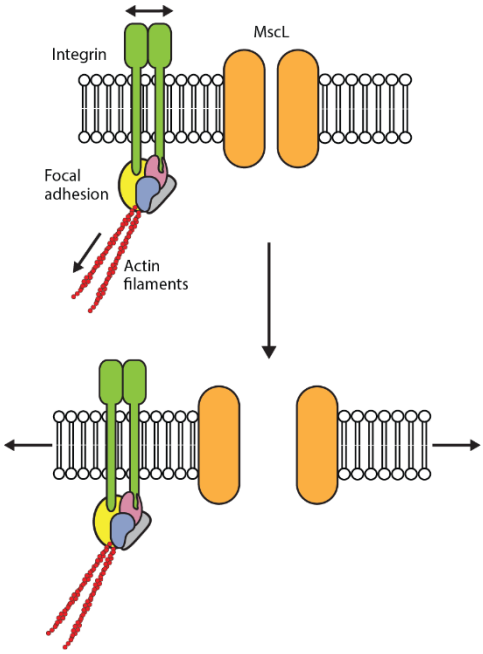

Figure 3.5 Postulated Model for Native Integrin-Actin Cytoskeleton and MscL Interaction in Mammalian Cells.

Having shown robust activation of MscL in mammalian cells due to osmotic down-shock and integrin-actin perturbation, we look into MscL's effect on cellular function – the output of mechanotransduction. We focus on cell migration in cancer

metastasis and then more specifically, 3D-confinements. During the physiological process of metastasis, cancer cells migrate through narrow pores and channels undergoing significant deformation[58, 59]. Moreover, in these 3D confined spaces cancer cells have been shown to utilize motility mechanism that rely on the actin-cytoskeleton and myosin[60], or native aquaporins and ion channels[61]. We hypothesize that functional MscL expression in these metastatic cancer cells in these contexts would lead to MscL activation and impairment of cancer cell migration.

CHAPTER IV

Expression of MscL in Mammalian Metastatic Cancer Cells for Study and Disruption of Migration in Narrow 3D Confinements

Introduction

Cancer metastasis, the migration and spread of cancer cells from primary tumors through the vasculature and lymphatic system to secondary tissues and organs, involves extreme physical deformation of tumor cells with cross-sectional areas of ~200 μm^2 through narrow paths and pores with cross-sectional areas of 10-300 μm^2 [59, 88, 89]. Such extreme deformation occurs mainly at the intravasation and extravasation steps and when migrating through dense regions of extracellular matrix in the metastatic cascade [90, 91]. Despite these apparently harsh physical obstacles on tumor cells, metastasis can persist, turning something like a non-life-threatening breast tumor into a multi-organ disease. This process of *in vivo* cancer cell migration and translocation continues to be the cause of an estimated 90% of cancer related fatalities [91-93].

The severe implications of metastasis have led to many investigations of cancer cell migration and development of various models of migration to help elucidate key aspects of metastasis. Emphasis of such research has diverted more and more from studying migration in 2D, planar environments where migration is dependent on

actin polymerization and polarization, Rho/ROCK myosin II contractility, integrin/matrix adhesion, and protrusion of lamellipodia type structures of the cell [94]. Work in 3D *in vitro* platforms, which aim to be more physiologically relevant, exhibit variability depending on the specific properties of the substrate and cell type. These migration models now incorporate not just the cytoskeleton components, but also metalloproteases, nucleoskeleton, intermediate filaments, and nuclear linker proteins [95-97].

Moreover, it has been recently demonstrated that cancer cell migration within confined 3-dimensional microfluidic channels is mediated by directional water permeation across the cell [61, 98, 99]. The over expression of aquaporins, AQ5, and sodium/hydrogen exchangers at the cell membrane, and their reorientation in cancer cells results in an "osmotic engine" propulsion system in which the cancer cells can have a net influx of water at their leading edge and net efflux of water at their trailing edge. This mode of migration was found to occur under extreme confinement, 30 μm^2, and is independent of cytoskeletal components [98], showing a novel model and mechanism for cancer cell migration and metastasis.

Previously, it was shown that an exogenous, bacterial channel protein, Mechanosensitive channel of large conductance (MscL), can be functionally expressed in mammalian cells [57, 62]. MscL is activated via membrane tension and deformation with a gating threshold of ~10.4 mN m^{-1} and gain of function mutant, MscL G22S with ~5-6 mN m^{-1} [22, 23, 43, 79]. MscL also has a large pore of ~3 nm diameter and is nonselective, allowing the bidirectional passage of any large osmolytes ≤ 10,000 Da

in size [51-53].The extreme deformation of the cancer cells through the metastatic cascade, in particular migration through narrow 3D confinements, is anticipated to result in MscL activation at the plasma membrane.

Here we hypothesize that MscL activation during the metastatic process will result in disruption and reduction of metastasis of tumor cells. To investigate MscL's effect on cancer metastasis and 3D confined migration, we developed stable metastatic breast cancer cell lines, MDA-MB-231, with gain of function mutant MscL G22S. We studied cell metastasis and primary tumor growth *in vivo* with an immunodeficient mice model and then, in greater detail, cancer cell migration in various channel cross-sections to mimic different degrees of confinement in an *in vitro* microfluidic platform.

Materials and Methods

Cells: MDA-MB-231 human breast cancer cells and 293T cells (ATCC) were cultured in DMEM (Thermo Fisher) with 10% bovine serum, 1% penicillin, streptomycin, and glutamine added in an incubator set to 5% CO_2 and 37°C.

Lentiviruses: A gene block with the sequence for MscL G22S fused to EGFP via a consensus cleavage sequence for TEV protease (IDT) was ordered and the DNA was inserted into the EcoRI and BamHI sites of the pLVX TetOne puromycin lentiviral vector (Takara). A gene block with optimized human codons for TEV protease (IDT) was ordered and this DNA was cloned into XbaI sites of lentiviral vector FUeqFP650. We generated lentiviruses in 293T cells as described.

In vivo Mouse Metastasis Experiments: MDA-MB-231 cells with doxycycline inducible expression of MscL G22S and constitutive click beetle green luciferase expression (231-MscL-CBG) and MDA-MB-231 cells with constitutive click beetle green luciferase-only (231-CBG) were injected bilaterally into 4th inguinal mammary fat pads of 6-10-week-old female NSG mice (Jackson Laboratory) on day 0. Three cohorts of mice were then studied: (1) 231-MscL-CBG mice treated with 1% sucrose in drinking water (n = 4); (2) 231-CBG mice with water containing 2 mg/ml doxycycline and 1% sucrose (n = 5); and (3) experimental group mice with 231-MscL-CBG cells and with water containing both doxycycline and sucrose as for group 2 (n = 5). Primary tumor size was tracked at the site of injection for each mouse via bioluminescence imaging (IVIS Spectrum, Perkin-Elmer). At day 43 the mice were euthanized and bioluminescence images of the liver, lung, spleen organs were taken to quantify metastases. Statistical significance testing of primary tumor growth data consisted of two-tailed student t-tests amongst all groups for each day. Statistical significance testing of the photon flux, metastasis data consisted of taking the log transform of all data points and performing a two-tailed t-test.

Stable Expression of MscL in MDA-MB-231 Cells: DNA constructs for the *E. coli* MscL WT were kindly provided by Boris Martinac (Victor Chang Cardiac Research Institute, Darlinghurst, Australia). The MscL WT construct was mutated to produce MscL G22S using a Q5® Site Direct Mutagenesis Kit (New England Biolabs, Ipswich, MA) and then subcloned into a lentiviral vector pLVX Puro (Takara Bio USA, Inc, Mountain View, CA). Lentivirus from constructs encoding only EGFP

(negative control, no MscL or EGFP-only) and EGFP-P2A-MscL G22S with FLAG tag inserted just after MscL residue I68 [100] were harvested from human embryonic kidney 293 T (HEK293T) cells. Metastatic breast cancer cells, MDA-MB-231, were transduced with either virus and maintained in RPMI 1640 supplemented with 10% fetal bovine serum, 10,000 units/mL of penicillin, 10,000 μg/mL of streptomycin, and 25 μg/mL of amphotericin B. For immunofluorescence imaging and flow cytometry analysis, MDA cells were fixed and permeabilized using methanol or fixed using 2% paraformaldehyde (PFA) for surface labeling with anti-FLAG iFluor 647 antibodies (Genscript, Piscataway, NJ). Analysis of infrared Western blots was conducted using a LI-COR Odyssey Sa system (Lincoln, Nebraska USA) and flow cytometry analysis was performed on a Millipore Sigma Guava® easyCyte flow cytometer (Burlington, MA).

MscL Osmotic-shock Functional Assay: MDA-MB-231 cells were suspended in solutions of varying osmolality containing 100 μM propidium iodide (PI) (Sigma-Aldrich, St. Louis, MO). PI is impermeable to the plasma membrane and label nucleic acids upon entering the cells. Prior to incubation, all cells were detached from culture dishes using 5 mM EDTA and counted using a Millipore Scepter™ to assure each bulk sample contained an equal number of cells of ~10^5. Sample fluorescence intensity due to PI uptake by the cells was measured using a Biotek Synergy H1 plate reader (Winooski, VT). Background fluorescence intensity was subtracted from data and values were normalized to the number of cells per bulk sample. Fluorescence

imaging of the samples was also performed on a Biotek Cytation 5 imaging plate reader and image processing was done using ImageJ (http://rsb.info.nih.gov/ij/).

In vitro Microfluidic Migration Device: The microfluidic device including 2D migration channels (cross-section: 50 μm x 10 μm and 20 μm x 10 μm) and narrow 3D constriction channels (cross-section: 10 μm x 10 μm, 6 μm x 10 μm, and 3 μm x 10 μm) was designed to be similar to previous migration devices [61, 99]. The device was designed to allow the chemoattractant gradient of fetal bovine serum (FBS) to be quickly established (~1hr) across all channels and that the gradient remained uniform and steady over the course of ~12 hrs, as verified through COMSOL Multiphysics (Burlington, MA) simulations. Soft lithography was used to fabricate the device out of polydimethylsiloxane (PDMS) (Dow Chemical, Midland, MI). The device design patterns were drawn in AutoCAD (San Rafael, CA) and printed onto a lithographic mask by CAD/Art Services (Bandon, OR, USA). The mask pattern was transferred onto SU-8 on a silicon wafer to produce the device mold for forming the PDMS cast. After punching inlets and outlets, the PDMS cast was then irreversibly bonded to a glass slide or coverslip following oxygen plasma treatment.

In vitro Migration Experiments: Assembled microfluidic migration devices were treated with 50 μg/mL of fibronectin (Sigma Aldrich, St. Louis, MO) in 1X PBS. The devices were then incubated for 1 hr at room temperature. After incubation, the devices were rinsed with 1X PBS and filled with phenol red-free RPMI 1640 media supplemented with 2% FBS and stored at 37° C. MDA cells were then detached from cell culture dishes using 5 mM EDTA and resuspended in phenol red-free RPMI 1640

media supplemented with 2% FBS and slowly pipetted into the cell inlet of the microfluidic migration device. Gravity driven flow, as a result of differential hydrostatic pressure in the device inlets and outlets, pushed the cells near the opening of the channels. Once a sufficient number of cells were at the entrance of the device channels, the gravity flow was removed by equalizing the height of the media in all inlets and outlets. The cells were incubated in the device for 30 minutes at 37° C and 5% CO_2 to allow them to adhere to the device bottom surface. Media was then gently removed from the chemoattractant inlet and replaced with media supplemented with 20% FBS. Migration devices were then mounted onto an Olympus spinning disk confocal microscope (Center Valley, PA). Time-lapse, Δt = 12 minutes, DIC and fluorescence images of cells in the devices were taken for 8-12 hrs on an Andor EMCCD camera using image acquisition software Metamorph.

Migration Tracking and Data Analysis: Time-lapse movies of cell migration in devices were first saved and organized using ImageJ software. For each movie, frame drift correction and manual cell position tracking were performed using MATLAB CellTracker [101]. All cells were binned into groups based on the width of the channel the cell travelled across. Cells were only tracked when fully inside of the channel and were tracked exclusively at the leading end. Average velocity for each cell was then calculated and the velocity distribution for each channel width was displayed using boxplots. Statistical significance testing of migration data consisted of two-tailed student t-tests of paired MscL G22S and no MscL groups for each channel width.

Results

Expression of Non-native Channel, MscL G22S, Impairs Metastasis to Mouse Lung: We first set out to test our hypothesis that expression of MscL G22S in metastatic cancer cells results in disruption of cell migration mechanisms and thus reduces metastasis by using an *in vivo* mouse model and doxycycline inducible expression system for MscL G22S in MDA-MB-231 cells [61, 99] (Figure 4.1). Here MDA-MB-231 cells express click beetle green (Cbg) luciferase for bioluminescence imaging of the cells and tumors within the mice. Some cells contain a doxycycline inducible expression vector for MscL G22S–TEV cleavable linker (TC)–EGFP. When TEV protease is constitutively expressed, it unlinks MscL G22S from EGFP to minimize EGFP's effect on MscL mechanosensitivity and function. Pre-TEV proteolysis MscL G22S is shown localizing to various cellular membranes and post-TEV proteolysis, EGFP is unlined and diffuse within the cell (Figure 4.1B, C). This was used to first determine MscL's localization in the MDA cells and then for our *in vivo* mouse experiments respectively.

Three cohorts of immunodeficient mice (1) injected with MDA-MB-231 MscL G22S luciferase cells given sucrose feed (2) injected with MDA-MB-231 luciferase only cells with doxycycline given sucrose feed, and experimental group (3) injected with MDA-MB-231 MscL G22S luciferase cells given doxycycline and sucrose feed (Figure 4.2A). Cohorts 1 and 2 were used to assess the effect of the non-induced MscL G22S construct and of doxycycline on the experimental results respectively. Luminescence imaging, used to track the primary tumor size change at the initial site of injection

over a period of ~5 weeks, showed no marked difference among the mouse cohorts suggesting that expression of MscL G22S had no significant effect on the development of the orthotopic tumor (Figure 4.2B). At the conclusion of the experiment the mice were euthanized and luminesce imaging was done of multiple organs to detect and quantify metastases (Figure 4.2C). The most notable finding is the reduced metastasis in the lung for cohort 3 relative to cohorts 1 and 2 (Figure 4.2D). This piece of evidence indicates that MscL G22S expression in metastatic breast cancer cells can impair metastasis. However, if the effect is due to specific disruption of cell migration in narrow 3D confinements cannot be discerned. For this, we study the cell migration using an *in vitro* microfluidic system that can mimic the narrow cross-sections we suspect are leading to MscL's ability to disrupt migration and metastasis.

Stable and Functional Expression of Bacterial MscL in MDA-MB-231: To eliminate the need for doxycycline induction, luciferase expression, and to have constitutive MscL expression, stable MDA-MB-231 EGFP (also referred to as no MscL) and EGFP-P2A-MscL G22S with FLAG-tag cell lines were generated using a lentiviral expression scheme (Figure 4.3A). Bicistronic expression of cytosolic EGFP and bacterial MscL G22S was achieved using a single DNA promoter and a P2A linker. When translated, a peptide bond at the end of the P2A linker fails to be made and thus the EGFP and MscL G22S proteins were expressed in immediate succession, but not as a single protein. Whole-cell western blot analysis using anti-FLAG showed robust expression of bacterial MscL G22S in the mammalian metastatic breast cancer cells (Figure 4.3B). In previous studies of MscL expressed in mammalian cells, MscL

localized to the cell plasma membrane as well as multiple membrane bound entities within the cell [57, 62]. Flow cytometry fluorescence intensity distributions for MDA MscL G22S with periplasmic FLAG-tag for fixed/permeabilized cells and fixed cells for surface labeling were both shifted towards the right compared to MDA no MscL cells indicating both intracellular and plasma membrane localization of MscL (Figure 4.3C). Direct comparison between the MDA MscL G22S permeabilized and surface labeling distributions showed that permeabilized cells had higher fluorescence inten-

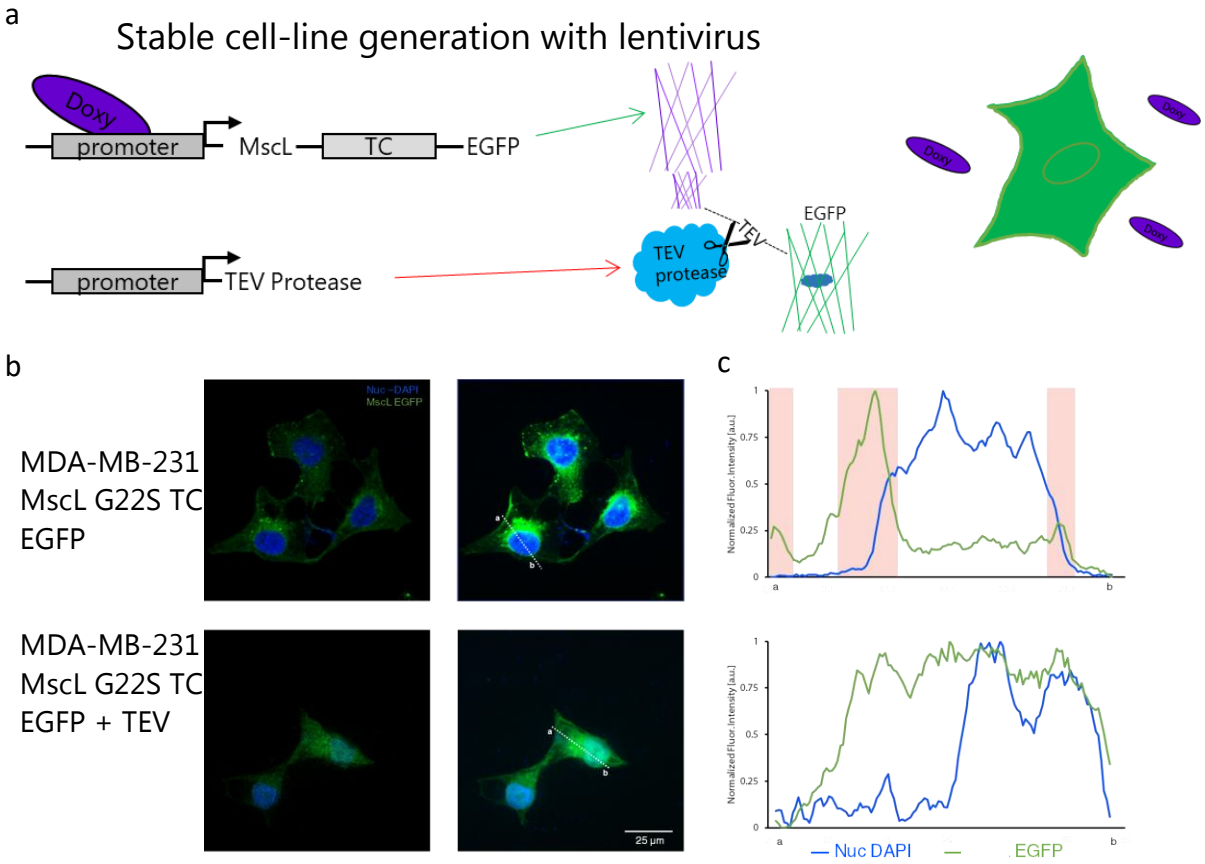

Figure 4.1 Doxycycline Inducible MscL-TC-EGFP Lentiviral Scheme for MDA MB 231. (A) Cells were co-transduced with a doxy inducible lentiviral vector encoding for MscL G22S-TEV Cleavable linker-EGFP and constitutive TEV protease vector. When TEV protease is co-expressed TC linker is hydrolyzed and MscL and EGFP are disconnected. (B) Fluorescence confocal images of MDA MB 231 MscL G22S EGFP cells without and with TEV expression (left panels: 1-imaging plane, right panels: z-stack superposition). (C) Graphs are fluorescence intensity profiles of DAPI and EGFP across line ab shown in the images. Without TEV, EGFP is bound to MscL G22S and has maximum fluorescence intensity/localization at the membranes (e.g., plasma membrane, ER, and nuclear membrane). With TEV expressed, EGFP is unbound, diffuse and cytosolic, not localizing to any specific area. Scale bar = 25 µm.

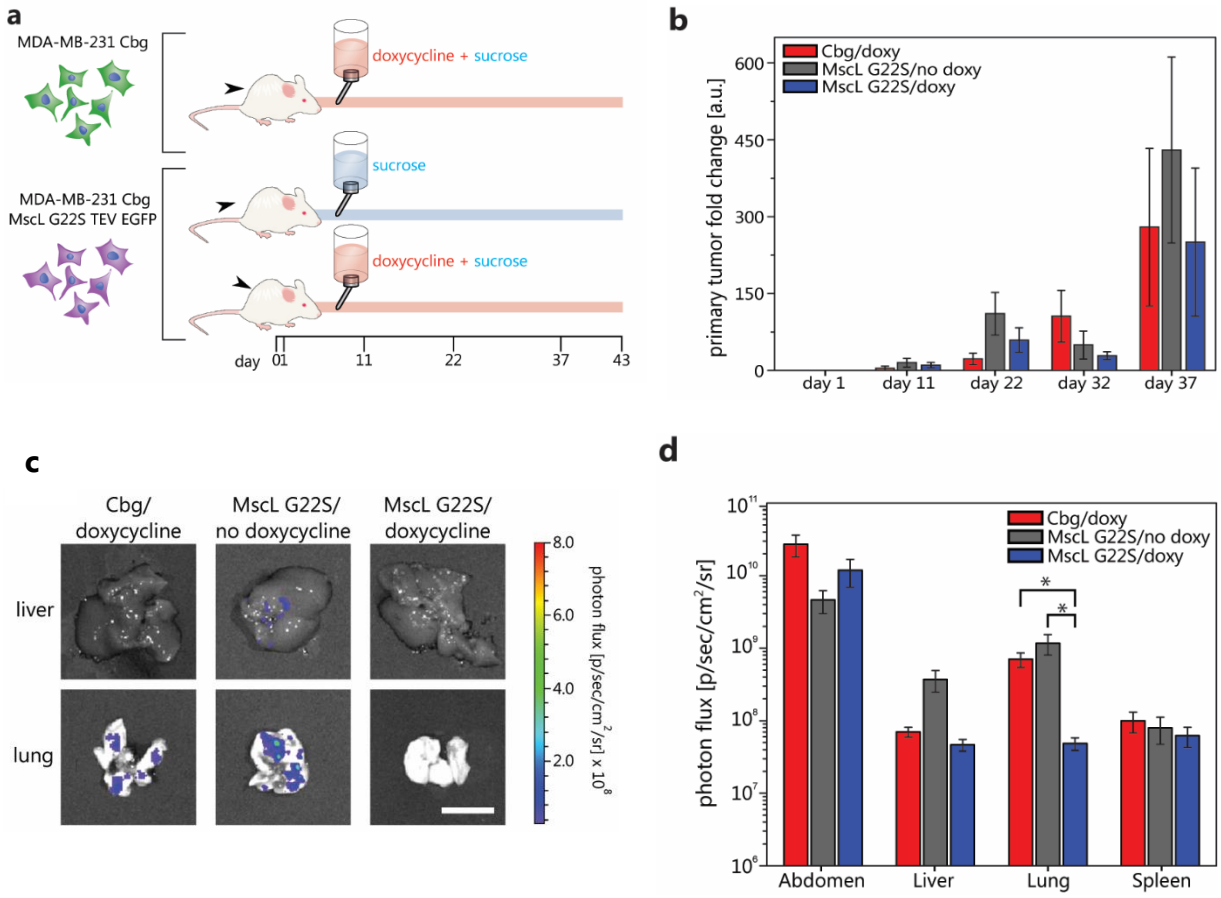

Figure 4.2 *In vivo* Experiment for Determining MscL's Effect on Cancer Cell Metastasis. (A) Cartoon description of *in vivo* experiments. MDA-MB-231 cells with doxycycline inducible expression of MscL G22S and constitutive luciferase expression and MDA cells with constitutive luciferase-only were injected under the mammary fat pad of immunodeficient mice on day 0. Three cohorts of mice were then studied, negative control groups (1) mice with MDA-MB-231 MscL G22S luciferase cells with sucrose feed (n = 4), (2) mice with MDA-MB-231 luciferase only cells with doxycycline and sucrose feed (n = 5), and experimental group (3) mice with MDA-MB-231 MscL G22S luciferase cells with doxycycline and sucrose feed (n = 5). (B) Average primary tumor size fold change at the site of initial injections as determined using bioluminescence imaging of mice on different days. Error bars are standard error of the mean. (C) Images of extracted liver and lung with luminesce signal false coloring and corresponding photon flux scale from a mouse of each cohort on day 43 relating to metastatic cancer cells at these secondary sites. Scale bar = 1 cm. Logarithmic plot of average luminescence signal, the result of metastatic cancer cells, described as photon flux for various organs of each cohort. Error bars represent the relative error of the mean. Vertical axis starts above luminescence background signal at $5x10^6$ p/sec/cm^2/sr. Two-tailed student t-test of log transformed data, *$p \leq 0.05$.

-sity and thus more labeling with anti-FLAG. Immunostaining of adherent permeabilized and surface labeled MDA MscL G22S cells reiterated these findings, showing that permeabilized cells had higher and more consistent labeling relative to surface labeled cells (Figure 4.3D).

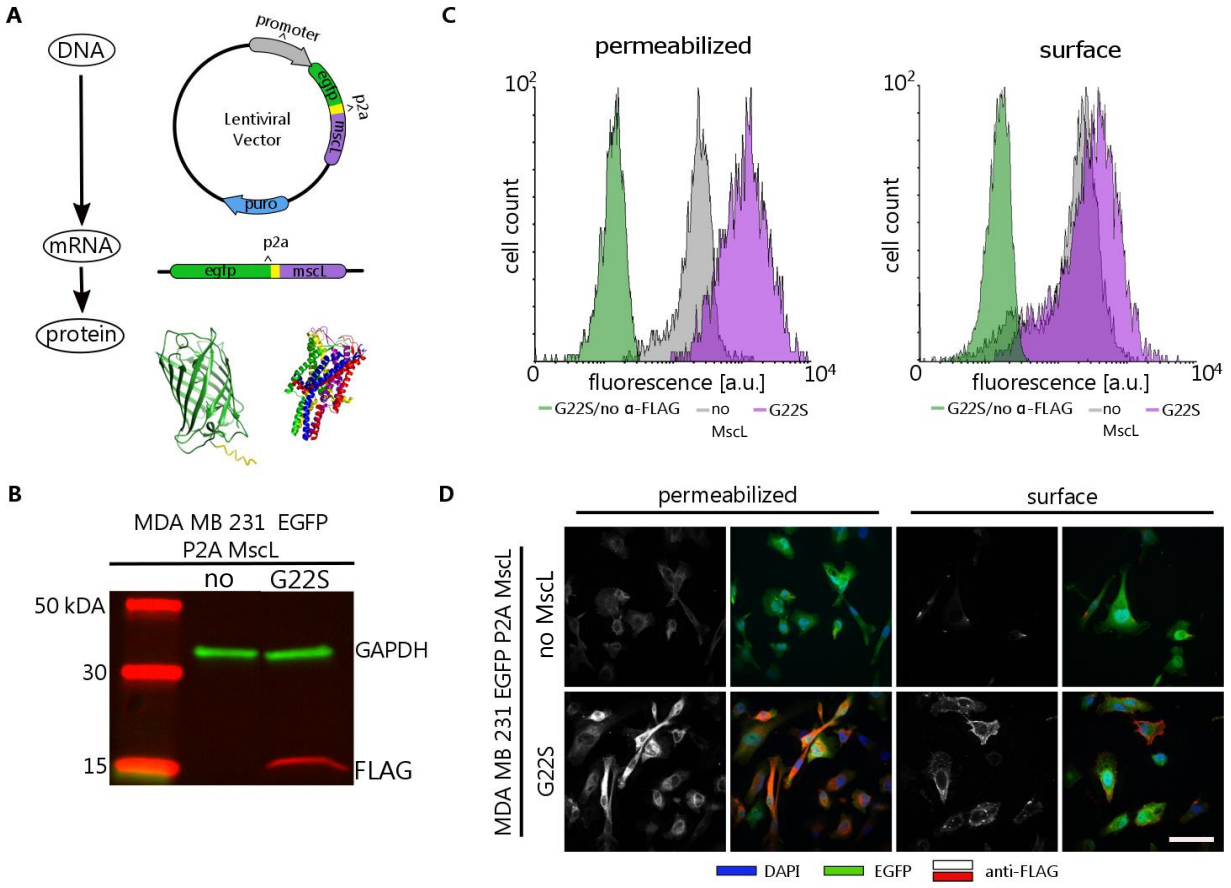

Figure 4.3 Viral Expression System for Constitutive Expression of MscL G22S in MDA-MB-231 Cells. (A) A single lentivirus vector system for bicistronic expression of cytosolic EGFP and MscL with single promoter. Downstream of the promoter, EGFP and MscL genes are encoded with a P2A linker sequence in between. The DNA for EGFP-P2A-MscL is transcribed into a single mRNA. Translation into protein results in an incomplete peptide bond of the P2A linker's final amino acid resulting in the expression of separate EGFP and MscL proteins. (B) Western blot analysis of transduced whole cells with negative control vector, no MscL EGFP-only, and experimental cells, EGFP-P2A-MscL G22S with periplasmic FLAG-tag. GAPDH was used as a housekeeping protein. (C) Flow cytometry fluorescence analysis using anti-FLAG Alexa Fluor® 647 of methanol fixed and permeabilized cells (left), and PFA fixed cells for surface analysis (right). Negative controls were EGFP-P2A-MscL G22S cells with no anti-FLAG and no MscL EGFP-only cells with anti-FLAG, and experimental cells were EGFP-P2A-MscL G22S with anti-FLAG. (D) Immunostaining of FLAG for no MscL EGFP-only cells (top) and EGFP-P2A-MscL G22S with FLAG-tag (bottom) with methanol permeabilization and fixation (2-left most panels) and PFA fixed cells for surface analysis (2-right most panels). DAPI was used to label cell nuclei. Scale bar = 25 μm.

An osmotic down-shock functional assay using impermeable dye, propidium iodide (PI), was performed on the MDA cells to determine if MscL mechanosensitive function was preserved and expression on the plasma membrane was sufficient for easily discernable mechanical activation as we have shown previously [62]. This functional assay capitalizes on the fact that in bacteria, MscL is hypothesized to

function as an emergency release valve that prevents cell lysis under osmotic down-shock by sensing increased membrane tension and allowing the flux of osmolytes across the bacterial cell inner membrane [102]. Simply, MscL in the mammalian cells was gated by osmotic down-shock (i.e., suspending the cells in solutions with osmolality much less than that inside of the cell) and fluorescence intensity from impermeable dye uptake was used to report MscL activation. The large size of MscL's open pore, ~30 Å, allows free passage of osmolytes ≤ 10 kDa [31, 57]. Propidium iodide, an impermeable molecule of 668.4 Da that intercalates in nucleotides, when unbound and in solution has excitation and emission peaks of 493nm and 636 nm respectively. Once PI is bound, its fluorescence intensity can increase 20- to 30-fold and excitation and emission peaks are shifted to 535 nm and 617 nm respectively. Confocal imaging of the MDA cells showed an increase in cell midplane cross-sectional area with decreasing osmolality: 1.92x fold for the 75 mmol/kg condition and 3.15x fold for 35 mmol/kg condition compared to the more iso-osmotic condition, 235 mmol/kg (Figure 4.4A, B) for MDA MscL G22S cells. MDA no MscL cells showed an increase in cell area with decreasing osmolality as well of 2.03x fold for the 75 mmol/kg condition and 2.87x fold for 35 mmol/kg condition compared to the more iso-osmotic condition, 235 mmol/kg (Figure 4.4C). The increase in cell cross-sectional area was caused by osmosis across the plasma membrane and into the cell. This swelling resulted in membrane tension sufficient for MscL gating and PI uptake. PI fluorescence intensity increased as the solution osmolality decreased (Figure 4.4D). The level of expression of MscL within the MDA cells allowed for significant differences in the measurable

PI uptake in MscL G22S expressing cells versus no MscL cells for the more extreme osmotic down-shock conditions 75 mmol/kg and 35 mmol/kg. All together, these results support that MscL G22S can be expressed and mechanically gated in metastatic breast cancer cells, MDA-MB-231.

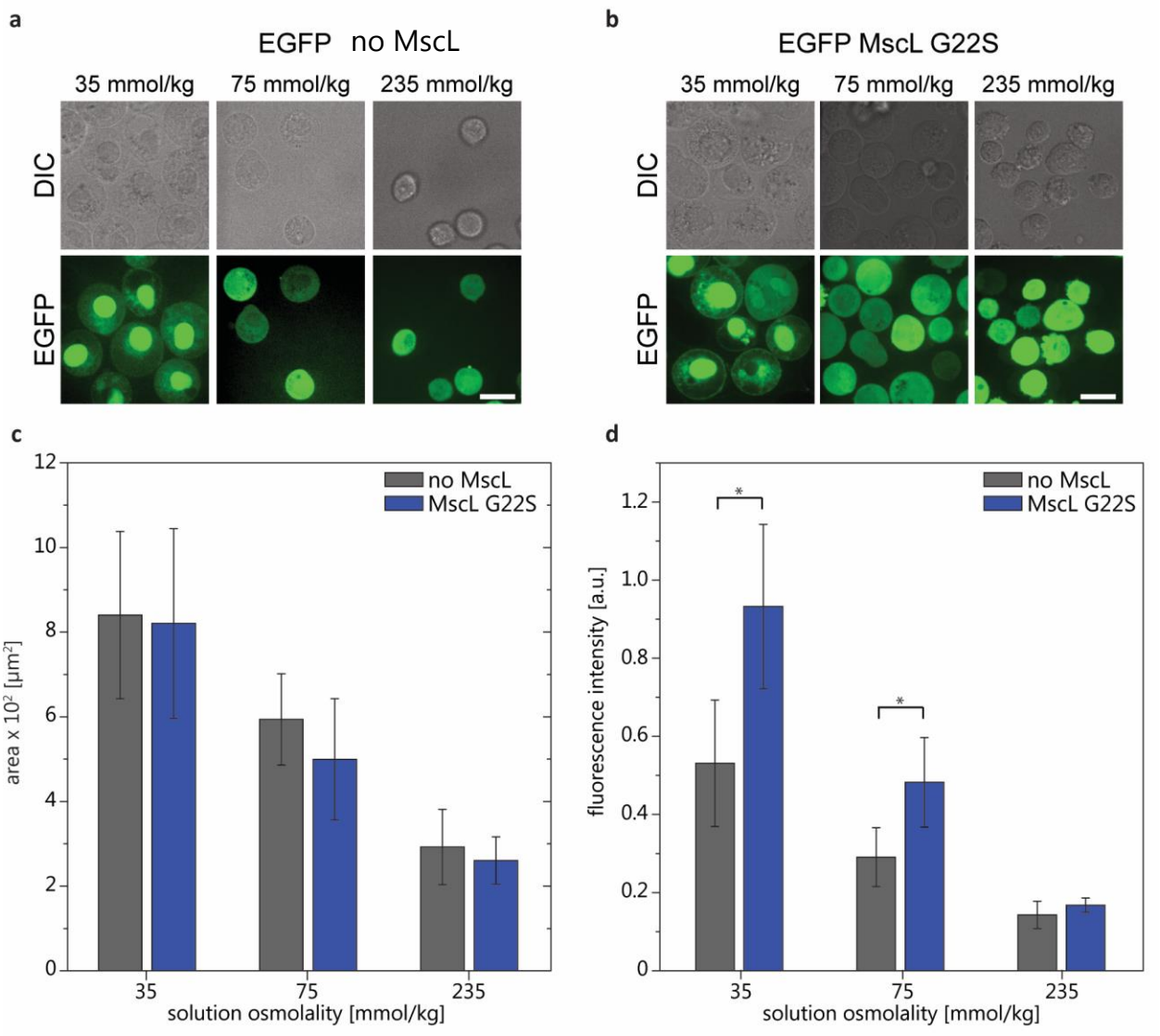

Figure 4.4 Osmotic Down-shock Functional Assay for MscL in MDA Cells. Phase and fluorescence confocal images of cells under suspended in solutions of varying osmolality (e.g., 235 mmol/kg ~ isotonic condition, 35 mmol/kg ~ hypotonic condition) with 100 μM of impermeable PI after 3 minutes of (A) MDA MscL G22S cells and (B) MDA no MscL cells. (C) Comparison of different cell type average area of cell midplane cross-section for different osmotic conditions. Inset is the comparison of same cell type average area for different osmotic conditions. (D) Average fluorescence intensity of PI uptake for cells in suspension under varying osmolality ($n_{cells} \approx 10^5$, $n_{exp} = 10$) for 6 minutes. Two-tailed student t-test *$p \leq 0.05$.

In vitro Microfluidic Migration Device with Narrow 3D Confinements: A microfluidic device was used to study the migration of the MDA cells in narrow confinements more robustly and precisely (Figure 4.5A). The device was designed to contain migration channels of varying cross-section for 2D, planar (channel widths: 20 and 50 μm) and narrow 3D confinement migration (channel widths: 3, 6, and 10 μm). Gravity driven flow was used to add cells to the device, situating them near the channel entrances, and to introduce a chemoattractant gradient that promoted cell chemotaxis across the channels. An FBS gradient was established quickly across all channels within 2 hrs and remained stable for >10 hours (Figure 4.5B). Confocal imaging showed that cells entered the different sized channels. Cells in the larger, 2D channels were not in contact will all of the channel walls, however cells in the narrower confinements appeared to completely "plug" the channels (Figure 4.5C). Cancer cell migration under this type of confinement has been shown to elicit and is required for the *osmotic engine* migration mechanism [61, 99]. Isometric volume views demonstrate the extent of cell deformation and conformation to the channel shape (Figure 4.5D).

Only Cancer Cells with Activated MscL G22S had Disrupted Migration in Narrow 3D Confinements: Our *in vivo* mouse experiments showed that introduction of MscL G22S into metastatic cancer cells led to impairment of metastasis to the lungs. By using the *in vitro* microfluidic migration device, we were able to ascertain if this outcome was a result of cell migration in narrow confinements. Phase and fluorescence time-lapse imaging of the cancer cells were used to determine the influe-

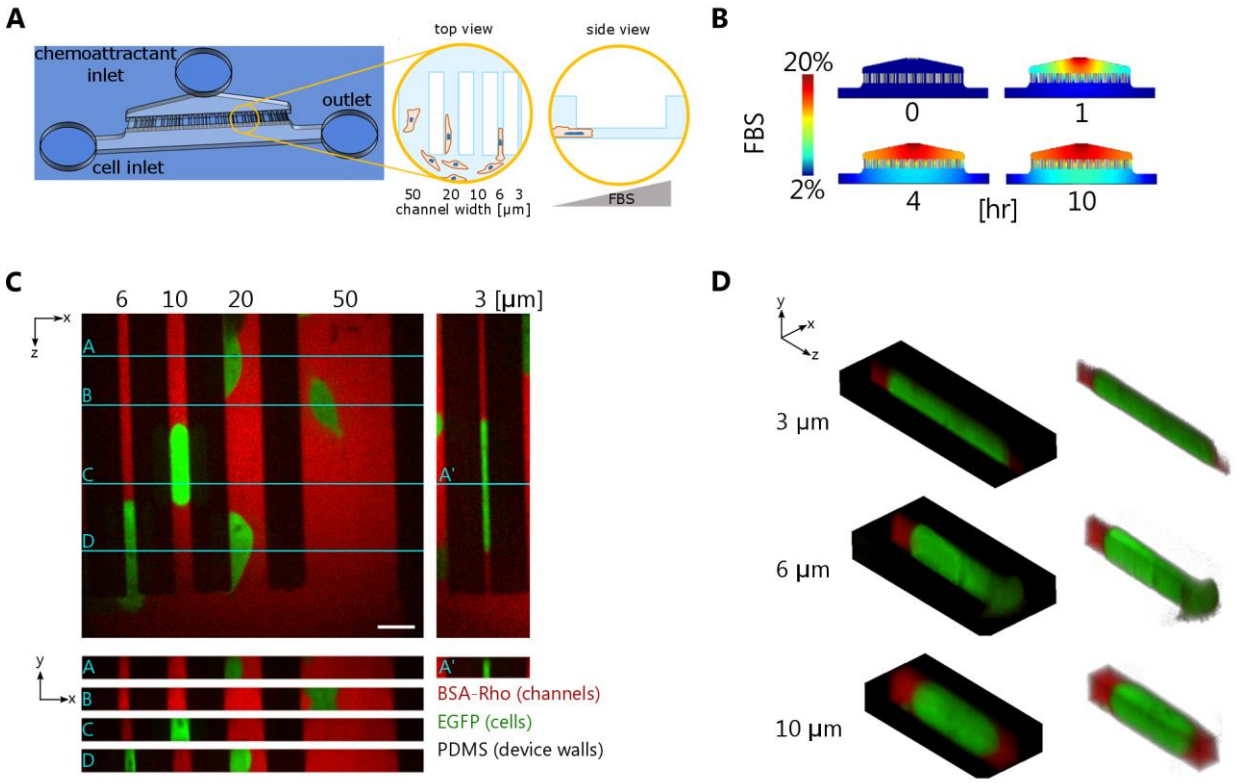

Figure 4.5 Microfluidic Platform for Study of Cancer Cell Migration Across 2D Channels and Narrow 3D Constrictions. (A) Cartoon of the PDMS microfluidic migration device. Cells are added to the device via a cell inlet and flow into the bottom section of the device, then they adhere to the glass substrate and migrate across channels of various sizes as a response to an FBS chemoattractant gradient as shown in the zoomed-in views. (B) Time-lapse images of multi-physics simulation of FBS gradient in the microfluidic device. (C) Fluorescence images showing orthogonal views, y-x and z-x, of cells in the microfluidic device channels. The z-x cross-sections of the labeled, turquoise lines on the y-x view are shown for cells in all channel widths. The PDMS/device walls appear black in the images, and the channels are filled with media containing BSA-rhomadime. Cells express cytosolic EGFP. Scale bar = 20 μm. (D) Isometric view of the cells in the narrow 3D constriction channels.

-nce of channel size and MscL G22S expression on cell migration. Cells migrated across the device in the direction of the chemoattractant gradient for ~10-12hrs and their change in position was manually tracked (Figure 4.6). Using PI during cell migration tracking showed a low proportion, 0-6%, of MscL G22S cells taking up dye when entering channels of 6, 10, 20, and 50 μm width (Figure 4.7A). In contrast, a larger proportion, 46.2%, of MscL G22S cells showed PI uptake when entering the narrowest channel of 3 μm width. Cell dye uptake was used as an indication of MscL

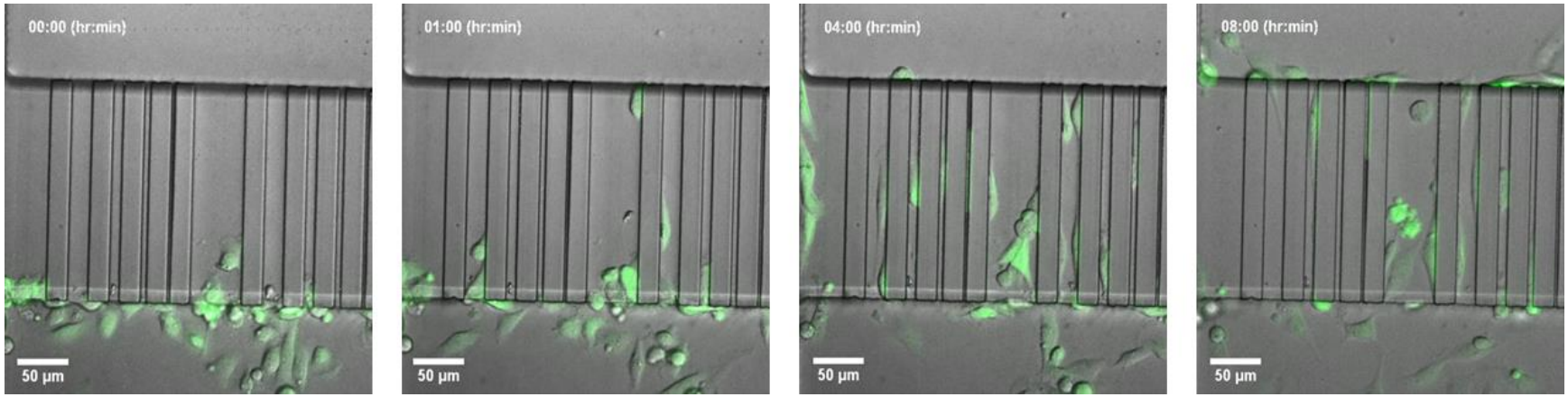

Figure 4.6 Time-lapse Microscopy Images of Migrating Cancer Cells in Microfluidic Device. MDA No MscL cells (green, EGFP) in migration device 0, 1, 4, and 8 hr. Scale bars = 50 µm

G22S activation in cells when migrating in the device. We found that the average cell velocity for the population of cells in the different sized channels decreased with narrower channel width for both no MscL and MscL G22S cells (Figure 4.7B-C). For MDA no MscL cells, the cell velocity from cell to cell varied more greatly for cells in the 10, 20, and 50 μm width channels, following a broader normal distribution of single cell velocity measurements. MDA no MscL cells in the 3 and 6 μm width channels had narrower velocity distributions (Figure 4.7B).

The velocity measurement distributions for MDA MscL G22S cells were consistently narrower (Figure 4.7C). Comparison of velocity of the no MscL and MscL G22S cells for 3D confined channel widths showed no statistically significant difference between the two cell types (Figure 4.7D). These results do not clearly indicate that MscL expression and potentially activation impair cancer cell migration in 3D narrow confinements. Revisiting our findings on MscL activation in the channels provided elucidation on this initially perceived discrepancy in our *in vivo* and *in vitro* results (Figure 4.7A).

Treating MscL G22S activated cells and MscL G22S non-activated cells that entered the 3 μm width channels as two separate populations showed that 87.5% (7 out of 8) of cells that successfully entered the channels and migrated (i.e., within a time frame of ~6hrs) did not have MscL activation. This in turn meant that only 12.5% of the 3 μm migrating MscL G22S cells were able to migrate. Our average velocity comparison between the no MscL and MscL G22S cells can then be inferred to have been appreciably influenced by the non-activated MscL G22S cells, resulting

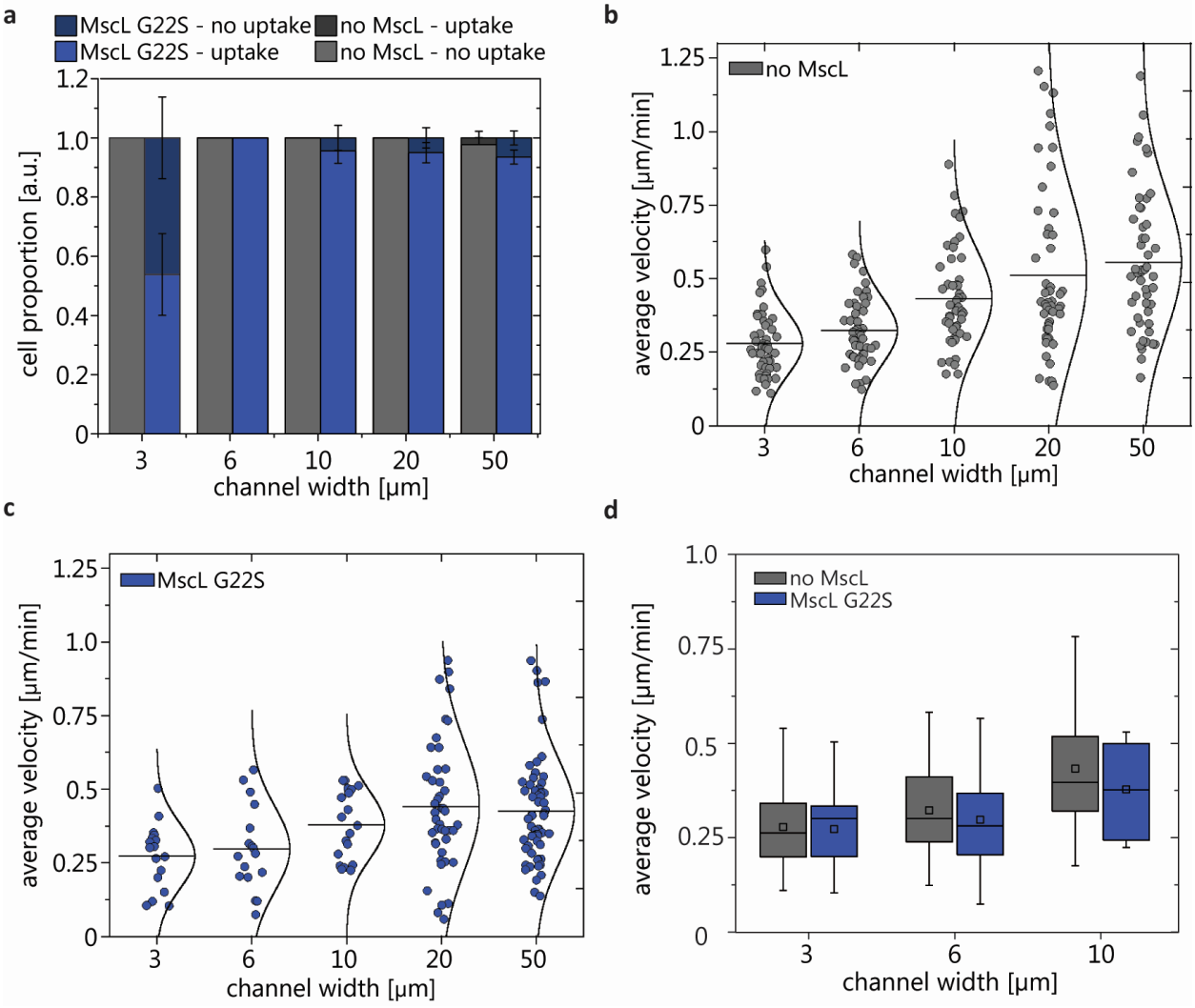

Figure 4.7 Analysis of Cancer Cell Migration *In vitro*. (A) Proportion of cells exhibiting PI uptake while entering or migrating across channels for different channel width. (B) Average velocity of MDA no MscL cells in the different sized channels of the microfluidic device. Circles represent average migration of individual cells; black bars are the average velocity for all cells for the given channel width and curves show a normal distribution for each group of cells. (C) Average velocity of MDA MscL G22S cells in the different sized channels of the microfluidic device. Circles represent average migration of individual cells; black bars are the average velocity for all cells for the given channel width and curves show a normal distribution for each group of cells. (D) Box plots of average cell migration for no MscL and MscL G22S cells in the different sized channels. Two-tailed student t-test, $^{**}p \leq 0.01$.

in similar average velocity, even in the narrow confinements. When restricting our analysis to MscL G22S activated cells, we found that ~89% (8 out of 9) of these cells were stuck at the 3 µm channel entrance, not migrating in the channels (Figure 4.8). These findings are more in alignment to what was observed from our *in vivo* model.

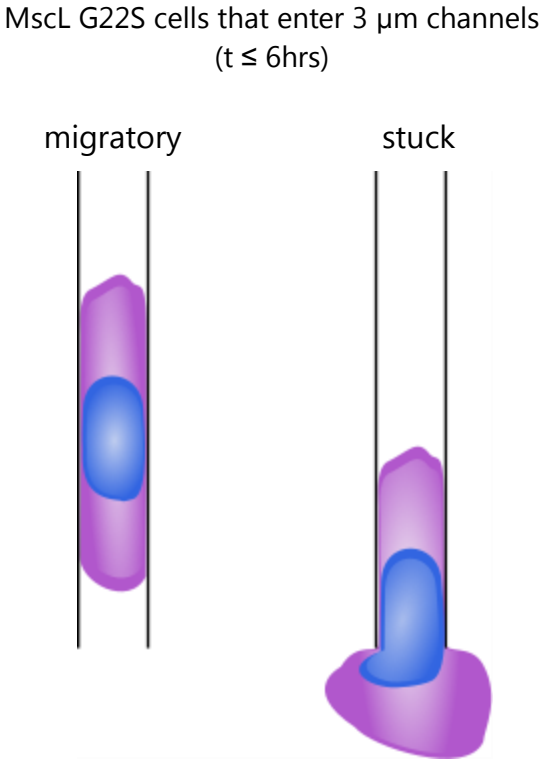

Figure 4.8 Cartoon Depicting Migratory and Stuck MDA MscL G22S Cells that Entered 3 μm Width Channels. Stuck cells represent cells that partially entered channels but were unable to fully enter the channels, remaining at the channel entrances for ~6 hrs.

Discussion

We were able to show that the expression of exogenous MscL G22S in metastatic breast cancer cells impaired metastasis to the lung of mice. However, when studying the cell migration *in vitro* the results suggest that migration of the MscL G22S cells and no MscL cells via narrow, 3D confinements are not different. However, MscL activation was observed for ~46% of cells the MscL G22S cells that were stuck or migrated across the 3 μm width channel. Of the total migratory cells, 87.5% were non-activated cells. Of the activated cells, ~89% were stuck and not migratory. This shows that if MscL G22S is activated, it can indeed impair cancer cell migration in 3D confinements. However, ~54% of MscL G22S cells did not exhibit

MscL G22S activation. This may be indicative of some unknown physiological factors not captured in our *in vitro* experiments such as osmotic variability, more complex topography or microenvironment more closely resembling the lung [103-105]. Incorporating this into our *in vitro* platform may result in higher cell proportions with MscL G22S activation and thus more cells becoming stuck.

Nevertheless, functional expression of an exogenous, mechanically gated channel such as MscL G22S resulted in reduced metastasis to the lung. Breast cancer has preferential metastasis to bone, lung, liver, and brain. The reasons for this have been linked to genetic influence leading to breast cancer subtypes that show metastatic variability but there is also physical factors that are becoming more apparent through research [88, 89, 106, 107]. Each of the organs have very distinct and different tissue architecture, mechanical properties, and composition yet breast cancer cells are able to metastasize to each one [108]. However, metastasis can be very different. For our own *in vivo* experiments, we were only able to perform necropsy on lung and liver, but already these two organs showed different results when compared to respective controls.

Given our findings, key next steps that can be taken to more precisely determine the cause of our finding for *in vivo* metastasis to lung would be redesigning a microfluidic platform with channels that have variable channel widths to better recapitulate the paths and pores encountered by the cells *in vivo*, incorporating a lung epithelium co-culture or means to trigger a phenotypic transition in the MDA cells[89, 108-110], or also varying solution osmolality while maintaining uniform

chemoattractant concentration. Investigating *in vivo* metastasis to other organs may be interesting as well to determine if the effect of MscL on cancer cell metastasis is lung specific or are the same results potentially observable in bone and brain.

Conclusions and Implications

We were able to demonstrate that MscL can be functionally expressed in metastatic cancer cells. MscL G22S expression in MDA-MB-231 cells was able to impair metastasis to lung in mice, *in vivo*. When investigating the role of 3D confinement on these results using an *in vitro* microfluidic device, our initial findings showed no marked difference in the average velocity of the no MscL and MscL G22S. However, more in-depth analysis showed that of the MscL G22S cells migrating in the narrowest confinement, 87.5% had non-activated MscL and of the active MscL G22S cells, ~89% became stuck. Taken together this shows that confined migration can result in MscL activation and this leads to impaired migration. However, MscL activation *in vivo* may not be solely due to 3D confined migration, needed further study.

Through our work we showed that MscL can be used to better understand or impair metastasis *in vivo*. And in our first studies, determine that straight channel, 3D confinement is not sufficient to recapitulate what occurs *in vivo;* and other factors are needed (e.g., channels with varying cross-section, 3D matrix, lung architecture or composition).

CHAPTER V

Conclusion & Future Work

In this thesis, it was shown that expression of bacterial MscL in mammalian cells endowed the cells with novel mechanotransduction capabilities, where we demarcate mechanotransduction as mechano-sensing of external mechanical forces, intercellular biochemical signaling, and altered cell function/behavior response. In particular, MscL conferred new mechano-sensing of membrane tension as a result of osmotic shock or integrin-actin linked ATC that led to channel activation and flux of molecules across the plasma membrane and altered cell function, the impairment of breast cancer metastasis to mice lung *in vivo* and migration in narrow 3D confined channels of 30 μm^2 cross-section *in vitro*.

These effects resulting from functional MscL expression were not exclusive to a single mammalian cell-line, but rather a variety of mammalian cells such as human retinal epithelial cells, Chinese hamster ovary cells, and MDA-MB-231metastatic breast cancer cells. This highlights MscL's applicability to many cell types that differ in phenotype such as epithelial versus mesenchymal, species origin, and healthy somatic cells versus cancer cells. For all of these cell lines MscL, was robustly expressed using standard adenoviral and lentiviral vectors and procedures. Optimization of the *mscL* gene was not necessary and constitutive expression did not negatively impact cell viability. High transduction efficiency and protein expression

were observed. This is perhaps attributed to MscL's relatively short genetic sequence and amino acid sequence, ~411 bp per subunit. Within each cell, MscL was also able to localize to multiple lipid membranes showing its potential as an intercellular probe or tool. Previous work has indicated that MscL does rely on lipid membrane composition, in particular mechano-sensing occurs when the membrane contains phosphatidylethanolamine (PE) [111, 112]. Whether this can impact MscL localization and function in mammalian cells, as lipid compositions from cell type to cell type and organelle to organelle[113], has not been investigated.

The osmotic down-shock functional assay was able to verify MscL mechano-sensing for these mammalian cell lines. Modifications to the assay, for example using fluorescence imaging for 2D substrate adherent cells and bulk fluorescence intensity measurements from a cell suspension for non-adherent cells, were successfully performed.

Ultimately here we have started to develop MscL's mechanotransduction repertoire and prove its versatility as a mechanobiology tool. We have already shown that MscL can be used as a tool for delivery of large, impermeable molecules into live cells using various types of mechanical stimulus. Our metastasis and migration studies have shown how MscL can provide insight into the metastatic cascade and, potentially, mechanobiology focused therapies. We hope that this work inspires further research utilizing MscL in mammalian cells to study existing mechanotransduction or potentially engineer new mechanical properties and/or signaling in cells, expanding the field of mechanobiology as we know it.

Future work involving MscL that can further this area of research would include studying our missing component of mechanotransduction: the effect of MscL activation on signaling pathways in cells and *vice versa*. Mechanotransduction pathways of interest would be Rho, Rac, and Cdc42 which are linked to proliferation,, survival, migration, and actin remodeling[114, 115]. This would also go hand-in-hand with studying MscL's influence on other cell functions.

MscL can also be reimagined to answer more sophisticated and difficult questions or accomplish better engineered mechanotransduction. For example, as mentioned previously, MscL localized to multiple membranes in mammalian cells. By fusing different leader sequences to MscL, the channel can be selectively trafficked to specific membranes within the cell[116, 117]. This can lead to more fine-tuned, subcellular study or effect of MscL mechanotransduction.

MscL can also be engineered to serve more literally as a tool for mechanobiology studies such as an *in-situ* membrane tension sensor. Plasma membrane tension is difficult to decouple from cortical tension and thus measure, often requiring use of optical tweezers[118]. Previous work focused on determining MscL open pore size and helix-tilt gating utilized Förster Resonance Energy Transfer (FRET)[31, 119, 120]. FRET signal from fluorophore tagged cysteine residues was used to correlate to MscL pore size. Given MscL's known open probability as a function of membrane tension, FRET signal can then be correlated to membrane tension. Finally, it would be interesting to see if MscL mechano-sensing can be enhanced through direct linkage to native mechanosensors such as the actin cytoskeleton. As

shown in our work, mechanical perturbation of integrins linked to actin led to MscL activation at the plasma membrane. One could expect that direct connection to the actin cytoskeleton could amplify the mechanical input sensed by MscL.

We have shown in this thesis, how bacterial MscL can be successfully expressed and mechanically gated in various mammalian cells, conferring these cells with novel, and desirable mechanotransduction. Therefore, we have demonstrated the potential for repurposing bacterial MscL for study in mammalian cells, both for more basic science and for applied research.

REFERENCES

1. Hynes RO (2004) The emergence of integrins: a personal and historical perspective. *Matrix biology : journal of the International Society for Matrix Biology* 23(6):333-340.
2. Kanchanawong P*, et al.* (2010) Nanoscale architecture of integrin-based cell adhesions. *Nature* 468(7323):580-584.
3. Berrier C, Coulombe A, Houssin C, & Ghazi A (1989) A patch-clamp study of ion channels of inner and outer membranes and of contact zones of E. coli, fused into giant liposomes. Pressure-activated channels are localized in the inner membrane. *FEBS letters* 259(1):27-32.
4. Martinac B, Buechner M, Delcour AH, Adler J, & Kung C (1987) Pressure-sensitive ion channel in Escherichia coli. *Proceedings of the National Academy of Sciences of the United States of America* 84(8):2297-2301.
5. Engler AJ, Sen S, Sweeney HL, & Discher DE (2006) Matrix elasticity directs stem cell lineage specification. *Cell* 126(4):677-689.
6. Huebsch N*, et al.* (2010) Harnessing traction-mediated manipulation of the cell/matrix interface to control stem-cell fate. *Nat Mater* 9(6):518-526.
7. Saha K*, et al.* (2008) Substrate modulus directs neural stem cell behavior. *Biophysical journal* 95(9):4426-4438.
8. Zarychanski R*, et al.* (2012) Mutations in the mechanotransduction protein PIEZO1 are associated with hereditary xerocytosis. *Blood* 120(9):1908-1915.
9. Glenister FK, Coppel RL, Cowman AF, Mohandas N, & Cooke BM (2002) Contribution of parasite proteins to altered mechanical properties of malaria-infected red blood cells. *Blood* 99(3):1060-1063.
10. Remmerbach TW*, et al.* (2009) Oral cancer diagnosis by mechanical phenotyping. *Cancer research* 69(5):1728-1732.
11. Sun Y, Chen CS, & Fu J (2012) Forcing stem cells to behave: a biophysical perspective of the cellular microenvironment. *Annual review of biophysics* 41:519-542.
12. Iskratsch T, Wolfenson H, & Sheetz MP (2014) Appreciating force and shape-the rise of mechanotransduction in cell biology. *Nature reviews. Molecular cell biology* 15(12):825-833.

13. Harris AK, Wild P, & Stopak D (1980) Silicone rubber substrata: a new wrinkle in the study of cell locomotion. *Science* 208(4440):177-179.

14. Oliver T, Dembo M, & Jacobson K (1995) Traction forces in locomoting cells. *Cell motility and the cytoskeleton* 31(3):225-240.

15. Moy VT, Florin EL, & Gaub HE (1994) Intermolecular Forces and Energies between Ligands and Receptors. *Science* 266(5183):257-259.

16. Rief M, Gautel M, Oesterhelt F, Fernandez JM, & Gaub HE (1997) Reversible unfolding of individual titin immunoglobulin domains by AFM. *Science* 276(5315):1109-1112.

17. Morimatsu M, Mekhdjian AH, Chang AC, Tan SJ, & Dunn AR (2015) Visualizing the interior architecture of focal adhesions with high-resolution traction maps. *Nano letters* 15(4):2220-2228.

18. Huang B, Bates M, & Zhuang X (2009) Super-resolution fluorescence microscopy. *Annual review of biochemistry* 78:993-1016.

19. Hur SC, Henderson-MacLennan NK, McCabe ERB, & Di Carlo D (2011) Deformability-based cell classification and enrichment using inertial microfluidics. *Lab Chip* 11(5):912-920.

20. Polacheck WJ, Li R, Uzel SG, & Kamm RD (2013) Microfluidic platforms for mechanobiology. *Lab Chip* 13(12):2252-2267.

21. Sukharev SI, Blount P, Martinac B, Blattner FR, & Kung C (1994) A large-conductance mechanosensitive channel in E. coli encoded by mscL alone. *Nature* 368(6468):265-268.

22. Sukharev SI, Martinac B, Arshavsky VY, & Kung C (1993) Two types of mechanosensitive channels in the Escherichia coli cell envelope: solubilization and functional reconstitution. *Biophysical journal* 65(1):177-183.

23. Chiang CS, Anishkin A, & Sukharev S (2004) Gating of the large mechanosensitive channel in situ: estimation of the spatial scale of the transition from channel population responses. *Biophysical journal* 86(5):2846-2861.

24. Chang G, Spencer RH, Lee AT, Barclay MT, & Rees DC (1998) Structure of the MscL homolog from Mycobacterium tuberculosis: a gated mechanosensitive ion channel. *Science* 282(5397):2220-2226.

25. Liu Z, Gandhi CS, & Rees DC (2009) Structure of a tetrameric MscL in an expanded intermediate state. *Nature* 461(7260):120-124.

26. Sukharev S, Betanzos M, Chiang CS, & Guy HR (2001) The gating mechanism of the large mechanosensitive channel MscL. *Nature* 409(6821):720-724.

27. Sukharev S, Durell SR, & Guy HR (2001) Structural models of the MscL gating mechanism. *Biophysical journal* 81(2):917-936.

28. Hase CC, Le Dain AC, & Martinac B (1997) Molecular dissection of the large mechanosensitive ion channel (MscL) of E. coli: mutants with altered channel gating and pressure sensitivity. *The Journal of membrane biology* 157(1):17-25.

29. Ou X, Blount P, Hoffman RJ, & Kung C (1998) One face of a transmembrane helix is crucial in mechanosensitive channel gating. *Proceedings of the National Academy of Sciences of the United States of America* 95(19):11471-11475.

30. Martinac B & Cox CD (2016) Mechanosensory Transduction: Focus on Ion Channels. *Reference Module in Life Sciences*, (Elsevier).

31. Wang Y*, et al.* (2014) Single molecule FRET reveals pore size and opening mechanism of a mechano-sensitive ion channel. *Elife* 3:e01834.

32. Ajouz B, Berrier C, Besnard M, Martinac B, & Ghazi A (2000) Contributions of the different extramembranous domains of the mechanosensitive ion channel MscL to its response to membrane tension. *The Journal of biological chemistry* 275(2):1015-1022.

33. Bavi N*, et al.* (2016) The role of MscL amphipathic N terminus indicates a blueprint for bilayer-mediated gating of mechanosensitive channels. *Nature communications* 7:11984.

34. Iscla I, Wray R, & Blount P (2008) On the structure of the N-terminal domain of the MscL channel: helical bundle or membrane interface. *Biophysical journal* 95(5):2283-2291.

35. Martinac AD*, et al.* (Structural Dynamics of the MSCL C-Terminal Domain. *Biophysical journal* 112(3):413a.

36. Kloda A, Ghazi A, & Martinac B (2006) C-terminal charged cluster of MscL, RKKEE, functions as a pH sensor. *Biophysical journal* 90(6):1992-1998.

37. Yoshimura K, Nomura T, & Sokabe M (2004) Loss-of-function mutations at the rim of the funnel of mechanosensitive channel MscL. *Biophysical journal* 86(4):2113-2120.

38. Yoshimura K, Batiza A, Schroeder M, Blount P, & Kung C (1999) Hydrophilicity of a single residue within MscL correlates with increased channel mechanosensitivity. *Biophysical journal* 77(4):1960-1972.

39. Bass RB, Strop P, Barclay M, & Rees DC (2002) Crystal structure of Escherichia coli MscS, a voltage-modulated and mechanosensitive channel. *Science* 298(5598):1582-1587.

40. Booth IR & Blount P (2012) The MscS and MscL families of mechanosensitive channels act as microbial emergency release valves. *Journal of bacteriology* 194(18):4802-4809.

41. Nomura T, Sokabe M, & Yoshimura K (2006) Lipid-protein interaction of the MscS mechanosensitive channel examined by scanning mutagenesis. *Biophysical journal* 91(8):2874-2881.

42. Sukharev SI, Sigurdson WJ, Kung C, & Sachs F (1999) Energetic and spatial parameters for gating of the bacterial large conductance mechanosensitive channel, MscL. *J Gen Physiol* 113(4):525-540.

43. Bartlett JL, Li Y, & Blount P (2006) Mechanosensitive channel gating transitions resolved by functional changes upon pore modification. *Biophysical journal* 91(10):3684-3691.

44. Li Y, Wray R, Eaton C, & Blount P (2009) An open-pore structure of the mechanosensitive channel MscL derived by determining transmembrane domain interactions upon gating. *FASEB journal : official publication of the Federation of American Societies for Experimental Biology* 23(7):2197-2204.

45. Perozo E, Cortes DM, Sompornpisut P, Kloda A, & Martinac B (2002) Open channel structure of MscL and the gating mechanism of mechanosensitive channels. *Nature* 418(6901):942-948.

46. Perozo E, Kloda A, Cortes DM, & Martinac B (2002) Physical principles underlying the transduction of bilayer deformation forces during mechanosensitive channel gating. *Nature structural biology* 9(9):696-703.

47. Kung C, Martinac B, & Sukharev S (2010) Mechanosensitive channels in microbes. *Annual review of microbiology* 64:313-329.

48. Haswell ES, Phillips R, & Rees DC (2011) Mechanosensitive Channels: What Can They Do and How Do They Do It? *Structure* 19(10):1356-1369.

49. Kloda A & Martinac B (2002) Common evolutionary origins of mechanosensitive ion channels in Archaea, Bacteria and cell-walled Eukarya. *Archaea* 1(1):35-44.

50. Pivetti CD*, et al.* (2003) Two families of mechanosensitive channel proteins. *Microbiology and molecular biology reviews : MMBR* 67(1):66-85, table of contents.

51. O'Hagan R, Chalfie M, & Goodman MB (2005) The MEC-4 DEG/ENaC channel of Caenorhabditis elegans touch receptor neurons transduces mechanical signals. *Nature neuroscience* 8(1):43-50.

52. Coste B*, et al.* (2010) Piezo1 and Piezo2 are essential components of distinct mechanically activated cation channels. *Science* 330(6000):55-60.

53. Christensen AP & Corey DP (2007) TRP channels in mechanosensation: direct or indirect activation? *Nature reviews. Neuroscience* 8(7):510-521.

54. Levina N*, et al.* (1999) Protection of Escherichia coli cells against extreme turgor by activation of MscS and MscL mechanosensitive channels: identification of genes required for MscS activity. *The EMBO journal* 18(7):1730-1737.

55. Sachs F & Morris CE (1998) Mechanosensitive ion channels in nonspecialized cells. *Reviews of physiology, biochemistry and pharmacology* 132:1-77.

56. Martinac B (1993) Mechanosensitive ion channels: biophysics and physiology. *Thermodynamics of Membrane Receptors and Channels* ed Jackson MB (Boca Raton: CRC Press), pp 327-351.

57. Doerner JF, Febvay S, & Clapham DE (2012) Controlled delivery of bioactive molecules into live cells using the bacterial mechanosensitive channel MscL. *Nature communications* 3:990.

58. Paul CD, Mistriotis P, & Konstantopoulos K (2017) Cancer cell motility: lessons from migration in confined spaces. *Nature reviews. Cancer* 17(2):131-140.

59. Wolf K*, et al.* (2009) Collagen-based cell migration models in vitro and in vivo. *Seminars in cell & developmental biology* 20(8):931-941.

60. Petrie RJ, Gavara N, Chadwick RS, & Yamada KM (2012) Nonpolarized signaling reveals two distinct modes of 3D cell migration. *The Journal of cell biology* 197(3):439-455.

61. Stroka KM*, et al.* (2014) Water permeation drives tumor cell migration in confined microenvironments. *Cell* 157(3):611-623.

62. Heureaux J, Chen D, Murray VL, Deng CX, & Liu AP (2014) Activation of a bacterial mechanosensitive channel in mammalian cells by cytoskeletal stress. *Cellular and molecular bioengineering* 7(3):307-319.

63. Lu Q (2005) Seamless cloning and gene fusion. *Trends in biotechnology* 23(4):199-207.

64. Hardy S, Kitamura M, Harris-Stansil T, Dai Y, & Phipps ML (1997) Construction of adenovirus vectors through Cre-lox recombination. *Journal of virology* 71(3):1842-1849.

65. Hase CC, Le Dain AC, & Martinac B (1995) Purification and functional reconstitution of the recombinant large mechanosensitive ion channel (MscL) of Escherichia coli. *The Journal of biological chemistry* 270(31):18329-18334.

66. van den Bogaart G, Krasnikov V, & Poolman B (2007) Dual-color fluorescence-burst analysis to probe protein efflux through the mechanosensitive channel MscL. *Biophysical journal* 92(4):1233-1240.

67. Levin G & Blount P (2004) Cysteine scanning of MscL transmembrane domains reveals residues critical for mechanosensitive channel gating. *Biophysical journal* 86(5):2862-2870.

68. Hayakawa K, Tatsumi H, & Sokabe M (2008) Actin stress fibers transmit and focus force to activate mechanosensitive channels. *Journal of cell science* 121(Pt 4):496-503.

69. Savage C*, et al.* (1989) mec-7 is a beta-tubulin gene required for the production of 15-protofilament microtubules in Caenorhabditis elegans. *Genes & development* 3(6):870-881.

70. Sokabe M, Sachs F, & Jing ZQ (1991) Quantitative video microscopy of patch clamped membranes stress, strain, capacitance, and stretch channel activation. *Biophysical journal* 59(3):722-728.

71. Fan Z*, et al.* (2013) Acoustic tweezing cytometry for live-cell subcellular modulation of intracellular cytoskeleton contractility. *Scientific reports* 3:2176.

72. White CR & Frangos JA (2007) The shear stress of it all: the cell membrane and mechanochemical transduction. *Philosophical transactions of the Royal Society of London. Series B, Biological sciences* 362(1484):1459-1467.

73. Singh A*, et al.* (2013) Adhesion strength-based, label-free isolation of human pluripotent stem cells. *Nature methods* 10(5):438-444.

74. Dayton PA*, et al.* (1997) A preliminary evaluation of the effects of primary and secondary radiation forces on acoustic contrast agents. *IEEE Transactions on Ultrasonics, Ferroelectrics, and Frequency Control* 44(6):1264-1277.

75. Marmottant P & Hilgenfeldt S (2003) Controlled vesicle deformation and lysis by single oscillating bubbles. *Nature* 423(6936):153-156.

76. Goertz DE, de Jong N, & van der Steen AFW (2007) Attenuation and size distribution measurements of definity and manipulated definity populations. *Ultrasound in medicine and biology* 33(9):1376-1388.

77. Fan Z, Liu H, Mayer M, & Deng CX (2012) Spatiotemporally controlled single cell sonoporation. *Proceedings of the National Academy of Sciences of the United States of America* 109(41):16486-16491.

78. Liu AP, Aguet F, Danuser G, & Schmid SL (2010) Local clustering of transferrin receptors promotes clathrin-coated pit initiation. *The Journal of cell biology* 191(7):1381-1393.

79. Haswell ES, Phillips R, & Rees DC (2011) Mechanosensitive channels: what can they do and how do they do it? *Structure* 19(10):1356-1369.

80. Chalfie M (2009) Neurosensory mechanotransduction. *Nature reviews. Molecular cell biology* 10(1):44-52.

81. Hochmuth RM (2000) Micropipette aspiration of living cells. *Journal of biomechanics* 33(1):15-22.

82. Nomura T*, et al.* (2012) Differential effects of lipids and lyso-lipids on the mechanosensitivity of the mechanosensitive channels MscL and MscS. *Proceedings of the National Academy of Sciences of the United States of America* 109(22):8770-8775.

83. Sukharev SI, Sigurdson WJ, Kung C, & Sachs F (1999) Energetic and spatial parameters for gating of the bacterial large conductance mechanosensitive channel, MscL. *J Gen Physiol* 113(4):525-540.

84. Xiong W*, et al.* (2012) TMHS is an integral component of the mechanotransduction machinery of cochlear hair cells. *Cell* 151(6):1283-1295.

85. Anishkin A & Kung C (2013) Stiffened lipid platforms at molecular force foci. *Proceedings of the National Academy of Sciences of the United States of America* 110(13):4886-4892.

86. Martinac B (2013) The ion channels to cytoskeleton connection as potential mechanism of mechanosensitivity. *Biochimica et biophysica acta*.

87. Sukharev S & Sachs F (2012) Molecular force transduction by ion channels: diversity and unifying principles. *Journal of cell science* 125(Pt 13):3075-3083.

88. Friedl P & Alexander S (2011) Cancer invasion and the microenvironment: plasticity and reciprocity. *Cell* 147(5):992-1009.

89. Wirtz D, Konstantopoulos K, & Searson PC (2011) The physics of cancer: the role of physical interactions and mechanical forces in metastasis. *Nature reviews. Cancer* 11(7):512-522.

90. Reymond N, d'Agua BB, & Ridley AJ (2013) Crossing the endothelial barrier during metastasis. *Nature reviews. Cancer* 13(12):858-870.

91. Chaffer CL & Weinberg RA (2011) A perspective on cancer cell metastasis. *Science* 331(6024):1559-1564.

92. Sporn MB (1996) The war on cancer. *Lancet* 347(9012):1377-1381.

93. Seyfried TN & Huysentruyt LC (2013) On the origin of cancer metastasis. *Critical reviews in oncogenesis* 18(1-2):43-73.

94. Doyle AD, Petrie RJ, Kutys ML, & Yamada KM (2013) Dimensions in cell migration. *Current opinion in cell biology* 25(5):642-649.

95. Aguilar-Cuenca R, Juanes-Garcia A, & Vicente-Manzanares M (2014) Myosin II in mechanotransduction: master and commander of cell migration, morphogenesis, and cancer. *Cellular and molecular life sciences : CMLS* 71(3):479-492.

96. Petrie RJ, Harlin HM, Korsak LI, & Yamada KM (2017) Activating the nuclear piston mechanism of 3D migration in tumor cells. *The Journal of cell biology* 216(1):93-100.

97. Petrie RJ, Koo H, & Yamada KM (2014) Generation of compartmentalized pressure by a nuclear piston governs cell motility in a 3D matrix. *Science* 345(6200):1062-1065.

98. Balzer EM*, et al.* (2012) Physical confinement alters tumor cell adhesion and migration phenotypes. *FASEB journal : official publication of the Federation of American Societies for Experimental Biology* 26(10):4045-4056.

99. Tong ZQ*, et al.* (2012) Chemotaxis of Cell Populations through Confined Spaces at Single-Cell Resolution. *PloS one* 7(1).

100. Kim JH*, et al.* (2011) High cleavage efficiency of a 2A peptide derived from porcine teschovirus-1 in human cell lines, zebrafish and mice. *PloS one* 6(4):e18556.

101. Piccinini F, Kiss A, & Horvath P (2016) CellTracker (not only) for dummies. *Bioinformatics* 32(6):955-957.

102. Levina N*, et al.* (1999) Protection of Escherichia coli cells against extreme turgor by activation of MscS and MscL mechanosensitive channels: identification of genes required for MscS activity. *Embo Journal* 18(7):1730-1737.

103. Jin Y, Ai J, & Shi J (2015) Lung microenvironment promotes the metastasis of human hepatocellular carcinoma cells to the lungs. *International journal of clinical and experimental medicine* 8(6):9911-9917.

104. Joyce JA & Pollard JW (2009) Microenvironmental regulation of metastasis. *Nature reviews. Cancer* 9(4):239-252.

105. Miller AJ & Spence JR (2017) In Vitro Models to Study Human Lung Development, Disease and Homeostasis. *Physiology (Bethesda)* 32(3):246-260.

106. DiMeo TA*, et al.* (2009) A novel lung metastasis signature links Wnt signaling with cancer cell self-renewal and epithelial-mesenchymal transition in basal-like breast cancer (vol 69, pg 5364, 2009). *Cancer research* 69(15):6366-6366.

107. Minn AJ*, et al.* (2005) Genes that mediate breast cancer metastasis to lung. *Nature* 436(7050):518-524.

108. Narkhede AA, Shevde LA, & Rao SS (2017) Biomimetic strategies to recapitulate organ specific microenvironments for studying breast cancer metastasis. *International journal of cancer* 141(6):1091-1109.

109. Furukawa M, Wheeler S, Clark AM, & Wells A (2015) Lung Epithelial Cells Induce Both Phenotype Alteration and Senescence in Breast Cancer Cells. *PloS one* 10(1).

110. Chaffer CL, Thompson EW, & Williams ED (2007) Mesenchymal to epithelial transition in development and disease. *Cells, tissues, organs* 185(1-3):7-19.

111. Lee AG (2004) How lipids affect the activities of integral membrane proteins. *Bba-Biomembranes* 1666(1-2):62-87.

112. Elmore DE & Dougherty DA (2003) Investigating lipid composition effects on the mechanosensitive channel of large conductance (MscL) using molecular dynamics simulations. *Biophysical journal* 85(3):1512-1524.

113. van Meer G & de Kroon AIPM (2011) Lipid map of the mammalian cell. *Journal of cell science* 124(1):5-8.

114. Wennerberg K & Der CJ (2004) Rho-family GTPases: it's not only Rac and Rho (and I like it). *Journal of cell science* 117(Pt 8):1301-1312.

115. Tapon N & Hall A (1997) Rho, Rac and Cdc42 GTPases regulate the organization of the actin cytoskeleton. *Current opinion in cell biology* 9(1):86-92.

116. Meyer GA & Radsak KD (2000) Identification of a novel signal sequence that targets transmembrane proteins to the nuclear envelope inner membrane. *Journal of Biological Chemistry* 275(6):3857-3866.

117. Choy E*, et al.* (1999) Endomembrane trafficking of Ras: The CAAX motif targets proteins to the ER and Golgi. *Cell* 98(1):69-80.

118. Diz-Munoz A, Fletcher DA, & Weiner OD (2013) Use the force: membrane tension as an organizer of cell shape and motility. *Trends in cell biology* 23(2):47-53.

119. Corry B, Rigby P, Liu ZW, & Martinac B (2005) Conformational changes involved in MscL channel gating measured using FRET spectroscopy. *Biophysical journal* 89(6):L49-L51.

120. Corry B*, et al.* (2010) An improved open-channel structure of MscL determined from FRET confocal microscopy and simulation. *J Gen Physiol* 136(4):483-494.